

Methane, carbon dioxide, and nitrous oxide emissions from two clear-water and two turbid-water urban ponds in Brussels (Belgium)

Thomas Bauduin ^{1,2}, Nathalie Gypens ¹, Alberto V. Borges ²

¹Ecology of Aquatic Systems, Université Libre de Bruxelles, Belgium

²Chemical Oceanography Unit, University of Liège, Belgium

Correspondence to: Thomas Bauduin (thomas.bauduin@ulb.be) and Alberto V. Borges (alberto.borges@uliege.be)

Abstract. Shallow ponds can occur either in a clear-water state dominated by macrophytes or a turbid-water state dominated by phytoplankton, but it is unclear if and how these two [alternative](#) states affect the emission to the atmosphere of greenhouse gases (GHGs) such as carbon dioxide (CO₂), methane (CH₄) and nitrous oxide (N₂O). We measured ~~on 46 occasions over 2.5 years (between June 2021 and December 2023)~~ the dissolved concentration of CO₂, CH₄, and N₂O from which the diffusive air-water fluxes were computed, in four urban ponds in the city of Brussels (Belgium): two clear-water macrophyte-dominated ponds (Silex and Tenreuken), and two turbid-water phytoplankton-dominated ponds (Leybeek and Pêcheres) [on 46 occasions over 2.5 years \(between June 2021 and December 2023\)](#). CH₄-~~ebullitive~~ [ebullitive](#) CH₄ fluxes were measured with bubble traps in the four ponds during deployments in spring, summer, and fall, totalling 48 days of measurements. ~~To characterize methanogenic pathways (acetoclastic or hydrogenotrophic) and quantify water column methane oxidation (MOX) we measured the ¹³C/¹²C ratio of CH₄ (δ¹³C-CH₄) from gas trapped in the bubble traps, from bubbles deliberately released by the perturbation of the sediments, and in dissolved CH₄ in the water column.~~ Measured ancillary variables included [water temperature](#), oxygen saturation level (%O₂), concentrations of chlorophyll-*a* (Chl-*a*), total suspended matter (TSM), soluble reactive phosphorus (SRP), nitrite (NO₂⁻), nitrate (NO₃⁻) and ammonium (NH₄⁺). The turbid-water and clear-water ponds did not differ significantly in terms of diffusive emissions of CO₂ and N₂O. Clear-water ~~(macrophyte-dominated)~~ ponds exhibited higher values of [annual ebullitive CH₄ fluxes](#) compared to turbid-water ~~(phytoplankton-dominated)~~ ponds, most probably in relation to the delivery ~~to sediments~~ of organic matter from macrophytes [to sediments, but the diffusive CH₄ emissions were not significantly different between clear- and turbid-water ponds. These findings imply that it might be necessary to account for the presence of submerged macrophytes when scaling ebullitive CH₄ fluxes in ponds at larger scale \(regional or global\) \(particularly if Chl-*a* is used as a descriptor\), although possibly less critical for diffusive CH₄, CO₂, and N₂O fluxes.](#) At seasonal scale, CH₄ emissions ~~exhibited a temperature dependence~~ [increased with water temperature](#) in all four ponds, with ebullitive CH₄ fluxes having a stronger dependence ~~to~~ [on water](#) temperature (*Q*₁₀) than diffusive CH₄ fluxes. The temperature sensitivity of ebullitive CH₄ fluxes decreased with increasing water depth, [implying that shallow sediments would respond more strongly to warming \(e.g. heat waves\).](#) ~~In summer, the δ¹³C-CH₄ values of sediment bubbles indicated that the hydrogenotrophic methanogenesis pathway seemed to dominate in clear water ponds and acetoclastic methanogenesis pathway seemed to dominate in turbid water ponds. The δ¹³C-CH₄ values of bubbles traps suggested a seasonal shift from the acetoclastic methanogenesis pathway in spring-summer to the hydrogenotrophic methanogenesis pathway in fall. The δ¹³C-CH₄ of dissolved CH₄ indicated higher rates of MOX in turbid water ponds compared to clear water ponds, with an overall positive correlation with TSM and Chl-*a* concentrations. The presence of suspended particles putatively enhanced MOX by reducing light inhibition of MOX and/or by serving as substrate in the water column for fixed methanotrophic bacteria.~~ Total [annual](#) CH₄ emissions (diffusive+ebullitive) in CO₂ equivalents ~~either equalled those of CO₂ in turbid-water ponds or and exceeded those of CO₂ those of CO₂ in clear-water ponds,~~ while N₂O emissions were negligible compared to the other two GHGs. Total annual GHG emissions in CO₂

equivalents from all four ponds increased from 2022 to 2023 due to higher CO₂ diffusive fluxes, likely driven by higher annual precipitation in 2023 compared to 2022 ([leading putatively to higher inputs for organic or inorganic carbon from runoff](#)), possibly in response to the intense El Niño event of 2023.

1. Introduction

Greenhouse gas (GHG) emissions from inland water (rivers, lakes, and reservoirs) to the atmosphere such as carbon dioxide (CO₂), methane (CH₄), and nitrous oxide (N₂O) are quantitatively important for global budgets (Lauerwald et al., 2023). GHG emissions from lakes are lower than from rivers for CO₂ (Raymond et al., 2013) and [for](#) N₂O (Lauerwald et al., 2019; Maavara et al., 2019). However, [reported](#) emissions of CH₄ from lakes (Rosentreter et al., 2021; Johnson et al., 2022) are [significant-equivalent or even higher](#) compared to rivers (Stanley et al., 2016; Rocher-Ros et al., 2023). Emissions of CO₂ and CH₄ from lakes to the atmosphere represent 1.25 to 2.30 Pg CO₂ equivalents (CO₂-eq) annually with a significant proportion from CH₄ emissions, and represent nearly 20% of global CO₂ emissions from fossil fuels (Delsontro et al., 2018). The contribution of CO₂ and CH₄ emissions from small lentic water bodies (small lakes and ponds) can be disproportionately high compared to large systems (Holgerson and Raymond, 2016) as small lakes and ponds are the most abundant of all water body types in number (Verpoorter et al., 2014; Cael et al., 2017), and [fluxes intensities](#) (per m²) are usually higher in smaller water bodies. The emissions of GHGs from artificial water bodies such as agricultural reservoirs, urban ponds, and storm-water retention basins could be higher than those from natural systems (Martinez-Cruz et al., 2017; Grinham et al., 2018; Herrero Ortega et al., 2019; Gorsky et al., 2019; Ollivier et al., 2019; Peacock et al., 2019, 2021; Webb et al., 2019; Bauduin et al., 2024). These higher emissions seem to result from higher external inputs of anthropogenic carbon and nitrogen [into](#) artificial systems, [e.g. with such as](#) rainfall runoff that brings organic matter and dissolved inorganic nitrogen (DIN), but might also reflect other differences compared to natural systems such as in hydrology (Clifford and Heffernan, 2018). Among artificial systems, urban ponds are the subject of a growing body of literature [on GHG emissions](#) (Singh et al., 2000; Natchimuthu et al., 2014; van Bergen et al., 2019; Audet et al., 2020; Peacock et al., 2021; Goeckner et al., 2022; Ray and Holgerson, 2023; [Ray et al. 2023](#); Bauduin et al., 2024). Urban areas can have numerous small artificial water bodies mostly associated to green spaces such as public parks, and their number is increasing due to rapid urbanisation worldwide (Brans et al., 2018; Audet et al., 2020; Gorsky et al., 2024; Rabaey et al., 2024). Urban ponds are generally small, shallow, and usually their catchment consists in majority of impervious surfaces with a smaller contribution from soils (Davidson et al., 2015; Peacock et al., 2021). [In general, the main function of urban ponds is for storm-water management but provide additional benefits including aesthetic/recreational amenities and habitats for wildlife \(e.g. Tixier et al., 2011; Hassall, 2014\).](#)

~~In shallow ponds and lakes, including urban ponds, aquatic primary production is either dominated by submerged macrophytes or by phytoplankton, corresponding to two alternate states (Scheffer et al., 1993). These occur in two alternative states corresponding to systems with either to clear waters (macrophyte-dominated) or turbid waters (phytoplankton-dominated), during the productive period of the year (spring and summer in mid-latitudes) (Scheffer et al., 1993). Submerged macrophytes and phytoplankton regulate CO₂ dynamics directly through photosynthesis that can be more or less balanced by community respiration in the water column (e.g., Sand-Jensen and Staehr, 2007). However, it is not clear whether the presence of macrophytes increases or decreases the net CO₂ emissions from ponds and lakes. Some studies have shown a decrease of CO₂ emissions with increasing macrophyte density (Kosten et al., 2010; Ojala et al., 2011; Davidson et al., 2015), but other studies showed the opposite pattern (Theus et al., 2023). In phytoplankton-dominated lakes, CO₂ concentrations depend in part on the developmental stage of the phytoplankton, with the growth and peak phases generally coinciding with lower CO₂ concentrations due to intense photosynthesis (Grasset et al., 2020; Vachon et al., 2020).~~

78 -CH₄ emissions have been reported to increase with the concentration of chlorophyll-*a* (Chl-*a*) in phytoplankton-dominated
 79 lakes (DelSontro et al., 2018; Borges et al., 2022). The presence of macrophytes strongly affects CH₄ cycling in freshwaters
 80 (Bastviken et al., 2023) and vegetated littoral zones of lakes exhibit higher CH₄ emissions than non-vegetated zones
 81 ([Hyvönen et al., 1998](#); [Huttunen et al., 2003](#); [Juutinen et al., 2003](#); Desrosiers et al., 2022; Theus et al., 2023). Macrophytes
 82 influence organic matter decomposition processes in sediments depending on the quality and quantity of plant matter they
 83 release into their environment (Reitsema et al., 2018; Grasset et al., 2019; Harpenslager et al., 2022; Theus et al., 2023). Yet,
 84 few studies have consistently compared CH₄ emissions in clear-water and turbid-water ponds (Hilt et al., 2017). A study in
 85 Argentina reported higher dissolved CH₄ concentrations in clear-water ponds with submerged macrophytes compared to
 86 turbid-water phytoplankton-dominated ponds, but no differences in measured CH₄ emissions (Baliña et al., 2023).

87 -The production of N₂O predominantly occurs through microbial nitrification and denitrification that depend on DIN- and O₂
 88 levels, [and temperature](#) (Codispoti and Christensen, 1985; Mengis et al., 1997; [Velthuis and Veraart, 2022](#)). Competition for
 89 DIN between primary producers and N₂O-producing microorganisms can impact N₂O production. Additionally, the transfer
 90 of labile phytoplankton organic matter to sediments fuels benthic denitrification [and impacts N₂O fluxes](#). [Eutrophication is](#)
 91 [assumed to drive high N₂O emissions from lakes and ponds](#) (Audet et al., 2020; Webb et al., 2021; Wang et al., 2021; Xie
 92 [et al., 2024](#)) but ~~Combined, these two processes could explain that some lakes with elevated Chl-*a* concentrations~~
 93 ~~act as sinks of N₂O due to removal of N₂O by denitrification under elevated Chl-*a* concentrations~~ (Webb et al., 2019; Borges
 94 et al., 2022; [2023](#)). The presence of macrophytes also strongly influences nitrogen cycling in sediments of lakes and ponds
 95 (Barko et al., 1991; Choudhury et al., 2018; Deng et al., 2020; Dan et al., 2021) and should in theory also affect N₂O
 96 emissions, although seldom investigated, and available studies provide contradictory conclusions. N₂O emissions ~~have~~
 97 ~~shown~~ to follow diurnal cycles of O₂ concentrations in areas dominated by submerged macrophytes in Lake Wuliangshui
 98 (China) (Ni et al., 2022) and the seasonal cycle of aboveground biomass of emerged macrophytes (*Phragmites*) in
 99 Baiyangdian Lake (China) (Yang et al., 2012). On the contrary, ~~some a study~~ies showed there ~~were~~-~~was~~ no significant
 100 differences of N₂O production in sediments of macrophyte-rich (n=10) and macrophyte-free (n=12) lakes in subtropical
 101 China (Liu et al., 2018). There ~~has~~ve been a very limited number of studies [systematically](#) investigating ~~systematically~~ how
 102 emissions differ between ponds dominated by phytoplankton and those dominated by macrophytes (~~Harpenslager et al.,~~
 103 ~~2022~~; Baliña et al., 2023), and none investigating simultaneously CO₂, CH₄, and N₂O emissions including both diffusive and
 104 ebullitive components.

105 The emissions from aquatic systems of CO₂ and N₂O are exclusively through diffusion across the air-water interface
 106 (diffusive flux), while CH₄ can be additionally emitted as bubbles released from sediments to the atmosphere (ebullitive
 107 flux). At annual scale, ebullitive CH₄ flux usually represents more than half of total (diffusive+ebullitive) CH₄ emissions
 108 from shallow lakes (Wik et al., 2013; Deemer and Holgerson, 2021), although the relative contribution of ebullitive and
 109 diffusive CH₄ emissions is highly variable seasonally (e.g. Wik et al., ~~2012~~3; Ray and Holgerson, 2023; [Rabaey and Cotner](#)
 110 [2024](#)). Ebullitive CH₄ fluxes are particularly high in the littoral zone of lakes at depths <5 m (Wik et al., 2013; DelSontro et
 111 al., 2016; Borges et al., 2022) and strongly increase in response to temperature (DelSontro et al., 2016; Aben et al., 2017;
 112 [Rabaey and Cotner 2024](#)), as well as organic matter availability (DelSontro et al., 2016; 2018). Ebullitive CH₄ fluxes tend to
 113 be higher in small and shallow water bodies (Deemer and Holgerson, 2021) but are notoriously variable in time and space,
 114 and are difficult to estimate reliably (DelSontro et al., 2011).

115 ~~The two primary metabolic pathways for CH₄ production in sediments by methanogenic archaea are the fermentation of~~
 116 ~~acetate (acetoclastic pathway) and the reduction of carbon dioxide by H₂ (hydrogenotrophic pathway) (Whiticar et al., 1986;~~

Conrad, 1989). CH_4 produced by these two pathways exhibits distinct $^{13}\text{C}/^{12}\text{C}$ ratios ($\delta^{13}\text{C}-\text{CH}_4$) (Whiticar et al., 1986) and can be used to discriminate which pathway is dominant. When CH_4 diffuses from sediments to the water column, it can be oxidized by methanotrophic bacteria who preferentially consume CH_4 with ^{12}C over ^{13}C , resulting in an increase of $\delta^{13}\text{C}-\text{CH}_4$ of the residual CH_4 in the water column (Bastviken et al., 2002). Fractionation models then allow estimating methane oxidation (MOX) from measurements of $\delta^{13}\text{C}-\text{CH}_4$ of dissolved CH_4 in the water column. Bastviken et al. (2008) report that 30 to 99% of the CH_4 produced in sediments of freshwater lakes can be removed by MOX that is as a significant CH_4 sink in these water bodies. MOX is known to be inhibited by light (Dumestre et al., 1998) and increases with the presence suspended particles (Abril et al. 2007) so that MOX might vary between clear and turbid waters (Morana et al. 2020).

Here, we report a dataset of CO_2 , CH_4 , and N_2O dissolved concentrations in four shallow and small urban ponds (Leybeek, Pêcherries, Silex, and Tenreuken) in the city of Brussels (Belgium) (Fig. 1), with data collected 46 times at regular intervals (between June 2021 and December 2023) on each pond. The air-water diffusive fluxes of CO_2 , CH_4 , and N_2O were calculated from dissolved concentrations and the gas transfer velocity, while the ebullitive CH_4 fluxes were measured with inverted funnels during 8 deployments (totalling 48 days) in the four ponds. The four ponds have similar depth, surface area, and catchment urban coverage, and mainly differ by the phytoplankton-macrophyte dominance, a clear-water state dominated by macrophytes and a turbid-water state dominated by phytoplankton (alternative states) (Fig. 1). The $\delta^{13}\text{C}-\text{CH}_4$ in the sedimentary bubbles and in the water provides additional information on CH_4 dynamics such as the methanogenesis pathway (acetoclastic or hydrogenotrophic) and MOX. We test whether the differences between the four ponds are explained by the differences between the two alternative states in terms of ~~We test the three hypotheses that the two alternative states drive differences in the four ponds of (i) is that the two alternative states in shallow lakes (a clear-water state dominated by macrophytes, or a turbid-water state dominated by phytoplankton) drive differences in the CO_2 , CH_4 , and N_2O dissolved concentration and diffusive emissions from the four studied artificial ponds, that have similar depth, surface area, and catchment urban coverage, and that mainly differ by the phytoplankton-macrophyte dominance; (ii). We also test the hypothesis that the two alternative states in shallow lakes drive differences in the ebullitive CH_4 emissions, water column MOX, and sedimentary methanogenesis pathway (acetoclastic or hydrogenotrophic) in the four studied ponds; (iii). relative contribution of CO_2 , CH_4 , and N_2O to the total GHG emissions in CO_2 -eq. The final objective of the present work is to determine the relative contribution of CO_2 , CH_4 , and N_2O to the total GHG emissions in CO_2 -eq and to test the hypothesis that the relative contribution of each GHG differs according to the two alternative states in shallow lakes.~~

2. Material and Methods

2.1. Field sampling and meteorological data

Sampling was carried out from a pontoon in the four ponds on the same day between 9am and 11am, 46 times on each pond between June 2021 and December 2023 at a frequency ranging from one (winter) to three (summer) times per month at a single fixed station in each of the four ponds. Water was sampled 5 cm below the surface with 60 ml polypropylene syringes for analysis of dissolved concentrations of CO_2 , CH_4 , and N_2O . Samples for CH_4 and N_2O were transferred from the syringes with a silicone tube into 60 ml borosilicate serum bottles (Wheaton-Weathon), preserved with 200 μl of a saturated solution of HgCl_2 , sealed with a butyl stopper and crimped with aluminium cap, without a headspace, ~~samples were~~ and stored at ambient temperature ~~protected from direct light~~ in the dark prior to analysis in laboratory. The partial pressure of CO_2 ($p\text{CO}_2$) was measured directly in the field, within 5 minutes of sample collection, with a Li-Cor Li-840 infrared gas analyser (IRGA) based on the headspace technique with 4 polypropylene syringes (Borges et al., 2019). A volume of 30 ml of sample water was equilibrated with 30 ml of atmospheric air within the syringe by shaking vigorously for 5 minutes. The headspace of

each syringe was then sequentially injected into the IRGA and a fifth syringe was used to measure atmospheric CO₂. The final pCO₂ value was computed taking into account the partitioning of CO₂ between water and the headspace, as well as equilibrium with HCO₃⁻ (Dickson et al., 2007) using water temperature measured in-situ and after equilibration, and total alkalinity (data not shown). Samples for total alkalinity were conditioned, stored, and analysed as described by Borges et al. (2019). The IRGA was calibrated in the laboratory with ultrapure N₂ and a suite of gas standards (Air Liquide Belgium) with CO₂ mixing ratios of 388, 813, 3788 and 8300 ppm. The precision of pCO₂ measurements was ±2.0%. Water temperature, specific conductivity, and oxygen saturation level (%O₂) were measured in-situ with VWR MU 6100H probe 5 cm below the surface. A 2 liter polyethylene water container was filled with surface water for conditioning the samples for other variables at the laboratory in Université Libre de Bruxelles.

Surveys to identify and quantify visually the relative coverage of emerged and submerged macrophytes were conducted in summer 2023 (Table S1). The resulting list of macrophyte species agreed with past studies in Brussels' ponds (Peretyatko et al., 2007).

Three bubble traps were deployed 50 cm apart for measuring ebullitive CH₄ flux. The bubble traps consisted of inverted polypropylene funnels (diameter 23.5 cm) mounted with 60 ml polypropylene syringes, with three way stop valves allowing to collect the gas without contamination from ambient air. The polypropylene funnel was attached with steel rods to a polystyrene float. The volume of gas collected in the funnels was sampled with graduated polypropylene 60 ml syringes every 24 hours. The value of the collected volume of gas was logged, and the gas was transferred immediately after collection to pre-evacuated 12 ml vials (Exetainers, Labco, UK) that were stored at ambient temperature ~~protected from direct light in the dark~~ prior to the analysis of CH₄ concentration and $\delta^{13}\text{C}-\text{CH}_4$ in the laboratory. The time-series of measurements ~~were was~~ longer at the Silex pond than the other three ponds, because the Silex pond is closed to the public during the week, while the other three ponds are open to the public all the time.

~~In summer 2023, the bubbles present in the sediment were directly collected with bubble traps by physically perturbing the sediment below the traps with a wooden rod. The gas collected in the funnels was stored in pre-evacuated 12 ml vials (Exetainers, Labco, UK) that were stored at ambient temperature protected from direct light prior to the analysis of $\delta^{13}\text{C}-\text{CH}_4$ in the laboratory. These samples are referred hereafter to as from "perturbed sediments." The samples collected in the bubble traps during the ebullition measurements are referred to as from "trapped bubbles."~~

Air temperature, precipitation, wind speed, and atmospheric pressure, were retrieved from <https://wow.meteo.be/en> for the meteorological station of the Royal Meteorological Institute of St-Lambert (50.8408°N, 4.4234°E) in Brussels, located between 2.5 and 5.0 km from the surveyed ponds. Air temperature, wind speed and atmospheric pressure were averaged over 24 h to obtain a daily mean value. Precipitation was integrated each day to obtain cumulated daily rainfall.

2.2. Laboratory analysis

2.2.1. Chlorophyll-*a*, total suspended matter, and dissolved inorganic nutrients

Water was filtered through Whatman GF/F glass microfiber filters (porosity 0.7 µm) with a diameter of 47 mm for total suspended matter (TSM) and Chl-*a*. Filters for TSM were dried in an oven at 50 °C and filters for Chl-*a* were kept frozen (-20 °C). The weight of each filter was determined before and after filtration of a known volume of water using an Explorer™ Pro EP214C analytical microbalance (accuracy ±0.1 mg) for determination of TSM concentration. Chl-*a* concentration was measured on extracts with 90% acetone by fluorimetry (Kontron model SFM 25) (Yentsch and Menzel, 1963) with a limit of

detection of 0.01 $\mu\text{g L}^{-1}$. Filtered water was stored frozen (-20 °C) in 50 ml polypropylene bottles for analysis of dissolved nutrients. Soluble reactive phosphorus (SRP) was determined by the ammonium molybdate, ascorbic acid and potassium antimony tartrate staining method (Koroleff, 1983), with a limit of detection of 0.1 $\mu\text{mol L}^{-1}$. Ammonium (NH_4^+) was determined by the nitroprusside-hypochlorite-phenol staining method (Grasshoff and Johannsen, 1972), with a limit of detection of 0.05 $\mu\text{mol L}^{-1}$. Nitrite (NO_2^-) and nitrate (NO_3^-) were determined before and after reduction of NO_3^- to NO_2^- by a cadmium-copper column, using the Griess acid reagent staining method (Grasshoff ~~et al.~~ and Kremling, 2009), with a detection limit of 0.01 and 0.1 $\mu\text{mol L}^{-1}$, respectively. Concentration of dissolved inorganic nitrogen (DIN) was calculated as the sum of NH_4^+ , NO_2^- and NO_3^- concentrations in $\mu\text{mol L}^{-1}$.

2.2.2. CH_4 and N_2O measurements by gas chromatography and $\delta^{13}\text{C}-\text{CH}_4$ by cavity ring down spectrometry

Measurements of N_2O and CH_4 concentrations dissolved in water and in the gas samples from bubbles were made with the headspace technique (Weiss, 1981) with an headspace volume of 20 ml of ultra-pure N_2 (Air Liquid Belgium) and a gas chromatograph (GC) (SRI 8610C) with a flame ionisation detector for CH_4 and an electron capture detector for N_2O calibrated with $\text{CH}_4:\text{N}_2\text{O}:\text{N}_2$ gas mixtures (Air Liquide Belgium) with mixing ratios of 1, 10 and 30 ppm for CH_4 , and 0.2, 2.0 and 6.0 ppm for N_2O . The precision of measurement based on duplicate samples was $\pm 3.9\%$ for CH_4 and $\pm 3.2\%$ for N_2O .

The CO_2 concentration is expressed as partial pressure (pCO_2) in parts per million (ppm) and CH_4 as dissolved concentration (nmol L^{-1}), as frequently used in topical literature. CH_4 concentration were systematically and distinctly above saturation level (2-3 nmol L^{-1}) and pCO_2 values were ~~only five times~~ below saturation ~~only five times~~ out of the 187 measurements. The N_2O concentrations fluctuated around atmospheric equilibrium, so data are presented as percent of saturation level ($\%\text{N}_2\text{O}$, where atmospheric equilibrium corresponds to 100%). The equilibrium with atmosphere for N_2O was calculated from the average air mixing ratios of N_2O provided by the Global Monitoring Division (GMD) of the National Oceanic and Atmospheric Administration (NOAA) Earth System Research Laboratory (ESRL) (Dutton and Hall, 2023), and using the Henry's constant given by Weiss and Price (1980).

~~The $\delta^{13}\text{C}-\text{CH}_4$ was measured in the gas of the headspace (20 ml of synthetic air, Air Liquid Belgium) equilibrated with the water sample (total volume 60 ml) for water samples and directly in the gas stored in Exetainers for samples from the bubble traps. The gas samples were diluted to obtain a final partial pressure of CH_4 in the cavity below 10 ppm (target value of 6 ppm) to fall within the operational concentration range of the instrument recommended by the manufacturer, prior to injection into a cavity ring down spectrometer (G2201i, Isotopic Analyzer, Picarro) with a Small Sample Introduction Module 2 (SSIM, Picarro). Data were corrected with curves of $\delta^{13}\text{C}-\text{CH}_4$ as a function of concentration based on two gas standards from Airgas Specialty Gases with certified $\delta^{13}\text{C}-\text{CH}_4$ values of $-23.9 \pm 0.3 \text{ ‰}$ and $-69.0 \pm 0.3 \text{ ‰}$.~~

2.3. Calculations

2.3.1. Diffusive GHG emissions

The diffusive air-water CO_2 , CH_4 , or N_2O fluxes (F_G) were computed according to:

$$F_G = k \times \Delta[G], \quad (1)$$

where k is the gas transfer velocity and $\Delta[G]$ is the air-water gas concentration gradient.

227 The atmospheric pCO₂ was measured in the field with the Li-Cor Li-840. For CH₄, the global average present day
 228 atmospheric mixing ratio of 1.9 ppm was used (Lan et al., 2024). Atmospheric N₂O concentration was calculated from the
 229 average air mixing ratios of N₂O provided by the GMD of the NOAA ESRL (Dutton et al., 2017). k was computed from a
 230 value normalized to a Schmidt number of 600 (k_{600}) and from the Schmidt number of CO₂, CH₄ and N₂O in freshwater
 231 according to the algorithms as function of water temperature given by Wanninkhof (1992). k_{600} was calculated from the
 232 parameterization as a function of wind speed of Cole and Caraco (1998). CH₄ and N₂O emissions were converted into CO₂
 233 equivalents (CO₂-eq) considering a 100-year timeframe, using global warming potentials of 32 and 298 for CH₄ and N₂O,
 234 respectively (Myrhe et al., 2013).

235 2.3.2. Ebullitive flux

236 Bubble flux (ml m⁻² d⁻¹) measured with the inverted funnels was calculated according to:

$$237 F_{bubble} = \frac{V_g}{A \times \Delta t}, \quad (2)$$

238 where V_g is the volume of gas collected in the funnels (ml), A is the cross-sectional area of the funnel (m²), Δt is the
 239 collection time (d).

240 A multiple linear regression model of F_{bubble} dependent on water temperature and drops of atmospheric pressure was fitted to
 241 the data according to:

$$242 \log_{10}(F_{bubble}) = \alpha \times T_w + \beta \times \Delta p + \gamma, \quad (3)$$

243 where α and β are the slope coefficients of the multiple linear regression model, γ is the y-intercept, T_w is the water
 244 temperature (°C), and Δp quantifies the drops in atmospheric pressure (atm), calculated according to Zhao et al. (2017):

$$245 \Delta p = -\frac{1}{\Delta t} \int_0^t p - p_0; \quad \forall p < p_0, \quad (4)$$

246 where p is the atmospheric pressure (atm), p_0 a threshold pressure fixed at 1 atm and Δt the time interval between two
 247 measurements (d) (Fig. S1).

248 Ebullitive CH₄ fluxes (mmol m⁻² d⁻¹) were calculated according to:

$$249 E_{CH_4} = [CH_4] \times F_{bubble}, \quad (5)$$

250 where $[CH_4]$ is the CH₄ concentration in bubbles (mmol ml⁻¹).

251 The methane ebullition Q_{10} represents the proportional change in the ebullitive CH₄ flux per 10°C change in water
 252 temperature (DelSontro et al., 2016) and was computed according to:

$$253 Q_{10} = 10^{10b}, \quad (6)$$

254 where b is the slope of the linear regression between the logarithm of the ebullitive CH₄ flux (E_{CH_4}) and T_w , and c is the y-
 255 intercept, according to:

$$256 \log_{10}(E_{CH_4}) = b \times T_w + c, \quad (7)$$

The flux of CH₄ from dissolution of rising bubbles was computed using the model of McGinnis et al. (2006) implemented in the SiBu GUI graphical user interface (Greinert and McGinnis, 2009).

Methane oxidation

The fraction of CH₄ oxidized (FOX) was calculated with a closed-system Rayleigh fractionation model (Liptay et al., 1998) according to:

$$\ln(1 - \text{FOX}) = \frac{\ln(\delta^{13}\text{C-CH}_4\text{-initial} + 1000) - \ln(\delta^{13}\text{C-CH}_4 + 1000)}{\alpha - 1}, \quad (8)$$

where $\delta^{13}\text{C-CH}_4\text{-initial}$ is the ¹³C/¹²C ratio of dissolved CH₄ as produced by methanogenesis in sediments, $\delta^{13}\text{C-CH}_4$ is the ¹³C/¹²C ratio of dissolved CH₄ in situ, and α is the fractionation factor.

We used a value of 1.02 for α based on laboratory culture experiments carried out at 26°C (Coleman et al., 1981) and field measurements in three Swedish lakes (Bastviken et al., 2002) and one tropical lake (Morana et al., 2015). The α values gathered in the three Swedish lakes were independent of season and temperature according to Bastviken et al. (2002).

For $\delta^{13}\text{C-CH}_4\text{-initial}$, we used a value of -69‰ for spring and summer, and -83‰ for fall based on average of measured $\delta^{13}\text{C-CH}_4$ in trapped bubbles (see Sect. 3.5). For winter we used a value of -76‰ corresponding to the average of the fall and spring/summer values.

MOX was computed from FOX and the F_G of CH₄ (F_{CH_4}) according to (Bastviken et al., 2002):

$$\text{MOX} = F_{\text{CH}_4} \times \frac{\text{FOX}}{1 - \text{FOX}}, \quad (9)$$

2.4. Statistical analysis

Statistical analysis was conducted with R version 4.4.1. Pearson's linear correlation coefficients and the r^2 coefficient were used to assess relationships between log-transformed variables within each pond and across the dataset, to identify potential pond-specific and overall direct relationships between variables and GHGs. Statistical significance was determined using Fisher's F test and the associated p -value. This approach was also applied to study the relationships between $\delta^{13}\text{C-CH}_4$, FOX and MOX with Chl a and TSM. To assess the impact of Chl a concentration, macrophyte cover in summer, water depth, and lake surface area on diffusive and ebullitive CH₄ fluxes, the ratio of ebullitive CH₄ to total CH₄ flux, and CO₂ and N₂O fluxes, both linear and quadratic relationships were applied to log-transformed averaged data. This approach allowed for the observation of trends between explanatory and dependent variables. For N₂O fluxes, additional explanatory variables included NO₂⁻, NO₃⁻, NH₄⁺, and DIN concentrations.

A two-way repeated measures analysis of variance (ANOVA) was used to test for differences in categorical variables, with the four seasons and the four ponds serving as independent factors, pond was set as a random effect to account for repeated measurements. A one-way repeated measures ANOVA was used to test for differences in $\delta^{13}\text{C-CH}_4$ from “perturbed sediments” with the four ponds serving as independent factors. After conducting an ANOVA and establishing significant differences among at least two groups ($p < 0.05$), Tukey's Honestly Significant Difference (HSD) post-hoc test was employed to perform pairwise comparisons across all groups. Statistical outcomes are visually represented on boxplots, where upper- and lower-case letters are used to denote significant differences ($p < 0.05$). Different lower- and upper-case letters indicate

significant differences between groups. Analyses were conducted using R version 4.4.1 (R Core Team, 2021). For the data-sets covering the whole sampling period, for pCO₂, dissolved CH₄ concentration, %N₂O, bubble flux, %CH₄ in bubbles, and both ebullitive and diffusive CH₄ fluxes, generalized linear mixed models (GLMMs) were constructed that included water temperature, rainfall, %O₂, Chl-*a*, TSM, DIN, SRP as fixed effects, and “pond” and “sampling date” as a random effect to account for repeated measurements via the *lme4* package (Bates et al., 2015) in R version 4.4.1 (R Core Team, 2021). When comparing data among the four ponds, “sampling date” was used as a random effect and post-hoc tests were performed using estimated marginal means (*emmeans* package) to assess pairwise differences between ponds.

For comparisons between the four seasons, When GLMMs did not converge due to insufficient number of data points, eComparisons on log-transformed data were then made using repeated measures Analysis of variance (ANOVA) with Tukey’s honestly significant difference (HSD) post-hoc tests and the effects of the measured variables on the response variables of interest were assessed using linear models on log-transformed data.

The relationships between the annual means of CH₄, CO₂ and N₂O fluxes and the annual means of a subset of variables (Chl-*a*, macrophyte cover, surface area, depth) were tested with Pearson’s linear or quadratic regressions. The modelled bubble fluxes in Silex pond were compared to measured values with Pearson’s linear regression.

Statistical significance was set at $p < 0.05$ for all analyses. For comparisons presented on boxplots, different lower-case letters indicate a significant difference between groups.

3. Results and discussion

3.1. Seasonal variations of meteorological conditions and GHG concentrations

The city of Belgium-Brussels has experiences a west-coast-marine temperate climate with mild weather year-round, and evenly distributed abundant rainfall totalling on average 837 mm annually for the reference period 1991-2020. The average annual air temperature was 11 °C, with summer average of 17.9 °C and winter average of 4.1 °C for the reference period 1991-2020. During the sampling period, from June 2021 to December 2023, water temperature in the surface of the four sampled ponds (Leybeek, Pêcherries, Silex, and Tenreuken; Fig. 1) tracked closely the air temperature that ranged between -1.5 and 30.0 °C following the typical seasonal cycle at mid-latitudes in the Northern Hemisphere (Fig. S2). Years 2022 and 2023 were about 1 °C warmer than the average for the period 1991-2020 (11 °C), while year 2021 was closer to the long-term average (Fig. 2). Year 2022 was warmer and drier than 2021 and 2023 (Fig. 2), with positive air temperature anomalies observed evenly throughout the year (9 months out of 12) and negative precipitation anomalies in summer, fall, and early winter (Fig. S2). Year 2021 had warmer and drier months in June and September, colder and wetter months in July and August, and was overall wetter and colder than 2022 (Fig. 2). Year 2023 was marked by both positive air temperature and precipitation anomalies (Fig. S2), resulting in a wetter and warmer year than normal and compared to 2021 and 2022 (Fig. 2). Daily wind speed was generally low ($<1 \text{ m s}^{-1}$) except for a windier period in spring 2022 (up to 5.8 m s^{-1} , corresponding to the Eunice storm) and in fall 2023 (up to 9.7 m s^{-1} , corresponding to the Ciarán storm) (Fig. S2).

The four sampled ponds are situated in the periphery of the city of Brussels, with the Silex pond bordered by the Sonian Forest (Fig. 1). The four ponds are relatively small (0.7-3.2 ha) and shallow (0.660-1.40 m) and have not been drained or dredged since at least 2018 (Table S2). The four studied ponds had significantly different Chl-*a* concentration values during summer, with the Leybeek pond having higher Chl-*a* ($78.8 \pm 49.5 \mu\text{g L}^{-1}$), followed by the Pêcherries pond ($19.1 \pm 13.7 \mu\text{g L}^{-1}$), the Tenreuken pond ($3.3 \pm 2.4 \mu\text{g L}^{-1}$), and the Silex pond ($1.0 \pm 1.2 \mu\text{g L}^{-1}$) (Tukey’s HSD test $p \leq 0.0001$ for Leybeek vs

~~Pêcheries, Leybeek vs Tenreuken, Leybeek vs Silex each pair of comparisons, Pêcheries vs Tenreuken, Pêcheries vs Silex, and $p=0.0052$ for Tenreuken vs Silex, Figs. 1, 3, Table S3). The Leybeek and Pêcheries ponds with higher summer Chl-*a* concentration had turbid-water (summer TSM = 48.7 ± 36.2 and 13.7 ± 10.7 mg L⁻¹, respectively), and undetectable submerged macrophyte cover in summer (Fig. 1, Table S1). The Tenreuken and Silex ponds with lower summer Chl-*a* concentrations had clear-water (summer TSM = 4.9 ± 3.2 and 4.0 ± 3.2 mg L⁻¹, respectively), and a high total macrophyte cover during summer (68 and 100%, respectively, Fig. 1, Table S1). Seasonally, the highest values of Chl-*a* were observed in summer ~~Values of Chl-*a* were higher in summer than in winter~~ in the turbid-water Leybeek and Pêcheries ponds, ~~(Tukey's HSD test $p=0.0107$ for the Leybeek pond, $p=0.0211$ for the Pêcheries pond)~~ related to summer algal blooms. Conversely, the lowest ~~y~~ Values of Chl-*a* were higher in winter than observed in summer in the clear-water Tenreuken and Silex ponds (Figs. 1, 3) ~~(Tukey's HSD test $=0.0296$ for the Tenreuken pond, $p=0.0056$ for the Silex pond)~~, probably related to competition for inorganic nutrients from macrophytes, ~~with the Silex pond showing lower summer Chl-*a* (Tukey's HSD test $p<0.0001=0.0052$), lower summer TSM concentrations (Tukey's HSD test $p<0.0001$) and higher summer total macrophyte cover compared to the Tenreuken pond (Figs. 1, 3).~~~~

The %O₂ values ranged from 11 to 191% (Fig. 3). The highest %O₂ values in the four ponds were observed in spring and summer compared to fall and winter owing to aquatic primary production. In summer, %O₂ was statically-significantly ~~higher~~ in the Leybeek pond ($109\pm46\%$) characterized by higher Chl-*a* concentration compared to the Pêcheries pond ($75\pm23\%$) ~~(Tukey's HSD test $p=0.0212$, Table S34037)~~. The lowest average %O₂ was observed in fall in the Pêcheries pond ($46\pm22\%$) and was significantly ~~statistically~~ lower than in the Leybeek ($85\pm34\%$, ~~Tukey's HSD test $p=0.0146$, Table S34302~~), Tenreuken ($76\pm26\%$, ~~Tukey's HSD test $p=0.0488$~~), and Silex ponds ($81\pm19\%$, ~~Tukey's HSD test $p=0.0130$, Table S3432~~). When data were pooled together, %O₂ was positively correlated to temperature. In individual ponds, %O₂ was positively correlated to temperature in the turbid-water Leybeek pond and in the clear-water Silex pond (Table S5).

The pCO₂ values ranged from 40 to 13,804 ppm (Fig. 3), ~~within the range of values typically observed in ponds (Holgerson and Raymond, 2016; Peacock et al., 2019; Audet et al., 2020)~~. Undersaturation of CO₂ with respect to atmospheric equilibrium was only observed on five occasions out of the 187 measurements, three times in the turbid-water Leybeek pond in summer (40 ppm on 13 August 2021, 220 ppm on 27 June 2022 and 149 ppm on 13 June 2023), and twice in the clear-water Tenreuken pond in spring and summer (383 ppm on 13 August 2021 and 55 ppm on 2 May 2022). Low values of pCO₂ were generally observed in spring and summer ~~probably due to uptake of CO₂ by primary production from either phytoplankton or submerged macrophytes. And~~ high values of pCO₂ were observed in fall in the four ponds ~~and probably reflect the release of CO₂ from degradation of organic matter due to the senescence of phytoplankton or macrophytes~~ (Fig. 3). In summer, pCO₂ was lower in the Leybeek pond (2187 ± 2012 ppm) than in the Pêcheries (3427 ± 1672 ppm, Tukey's HSD test $p=0.0015$, Table S34), and Silex (3222 ± 1175 ppm, Tukey's HSD test $p=0.0002$, Table S34) ponds and Tenreuken (2606 ± 1795 ppm, Tukey's HSD test $p=0.0879$, Table S34) ponds. When data were pooled together, pCO₂ was negatively correlated negatively correlated with %O₂, and, A general control of pCO₂ by biological activity (primary production and respiration) was confirmed by the strong negative correlation with %O₂ observed in all four ponds (e.g. Holgerson, 2015), as well as a positive correlation positively with both ~~correlated with~~ DIN observed in three ponds, and a positive correlation with positively correlated with SRP, and observed in the two clear-water ponds (Table S63; Figs S3, S4, S5, S6), confirming a general control of pCO₂ by biological activity (primary production and respiration) (e.g. Holgerson, 2015). A negative correlation between pCO₂ and Chl-*a* was only observed in the turbid-water Leybeek pond (Table S3; Fig S5), which showed the highest average Chl-*a* concentration, and no correlation was found in clear-water ponds, where aquatic primary production was presumably mainly related to submerged macrophytes (Table S3; Figs S3, S4). When data

were pooled together. In all four ponds, pCO_2 also strongly positively correlated positively to with precipitation (Table S463; Figs S3, S4, S5, S6) suggesting a control of external inputs of carbon either as organic carbon sustaining internal degradation of organic matter or as soil CO_2 (e.g. Marotta et al., 2011). In individual ponds, pCO_2 correlated negatively with $\%O_2$ and positively to with precipitations in the four ponds, positively with DIN in the Leybeek pond and Tenreuken ponds, and positively with DIN and SRP in the Tenreuken pond, and negatively with Chl-*a* in the Silex pond (Table S57).

The CH_4 dissolved concentrations ranged from 194 to 48,380 $nmol\ L^{-1}$ (Fig. 3) and was always above saturation, within the range of values typically observed in ponds (Holgerson and Raymond, 2016; Peacock et al., 2019; Audet et al., 2020). High values of CH_4 dissolved concentrations were generally observed in spring and summer and low values of CH_4 dissolved concentrations were generally observed in winter in the four ponds (Fig. 3). Dissolved CH_4 concentration was positively correlated to with water temperature in all four ponds (Table S3; Figs S3,S4,S5,S6), most probably reflecting the increase of sedimentary methanogenesis with temperature (Schulz and Conrad, 1996), with higher dissolved CH_4 concentrations observed in spring ($3160 \pm 5989\ nmol\ L^{-1}$) and summer ($3979 \pm 2993\ nmol\ L^{-1}$) than in fall ($2645 \pm 7315\ nmol\ L^{-1}$) and winter ($868 \pm 601\ nmol\ L^{-1}$) (Tukey's HSD test: spring versus fall, $p=0.0954$; spring versus winter, $p<0.0001$; summer versus fall, $p=0.0154$; summer versus winter, $p<0.0001$). In summer, CH_4 dissolved concentration was higher in the Silex pond ($4898 \pm 3384\ nmol\ L^{-1}$) than in the Pêcherries ($2518 \pm 2105\ nmol\ L^{-1}$, $p=0.0385$, Table S34) and Tenreuken ($2189 \pm 1365\ nmol\ L^{-1}$, $p=0.0055$, Table S34) ponds. When data were pooled together, dissolved CH_4 concentration was positively correlated with water temperature (Table S46). In individual ponds, dissolved CH_4 dissolved concentration was positively correlated with water temperature in the four ponds (Table S57). Additionally, CH_4 dissolved concentration was correlated positively with precipitation in the Leybeek pond, negatively with DIN in the Pêcherries pond, negatively with Chl-*a* in the Tenreuken pond, and negatively with Chl-*a* and positively with SRP in the Silex pond. Additionally, CH_4 dissolved concentration was correlated positively correlated with precipitation in the Leybeek pond and with SRP in the Silex pond, and negatively correlated to with precipitation and DIN in the Pêcherries pond (Table S3; Fig S6), and negatively correlated and with Chl-*a* in the Tenreuken pond, and positively correlated to SRP in the Silex pond (Table S3; Fig S457). These relationships between CH_4 and other variables probably indirectly reflect the seasonal variations of these other variables that showed correlations also correlated with water temperature, as DIN was negatively correlated negatively to with water temperature in the Pêcherries pond ($r^2=0.11$, $p=0.0028$), Chl-*a* was negatively correlated with temperature in the Tenreuken and Silex ponds, and SRP was positively and Chl-*a* negatively correlated to with water temperature in the Silex pond (Table S65) ($r^2=0.10$, $p=0.0103$). Dissolved CH_4 concentration was negatively correlated to with Chl-*a* in the Silex pond (Table S3; Fig S4) and to TSM in the Tenreuken pond (Table S3; Fig S3). These relationships probably reflect the negative relationship between Chl-*a* and temperature in the Silex pond ($r^2=0.13$, $p=0.0008$) and the negative relationship between TSM and temperature in the Tenreuken pond ($r^2=0.36$, $p<0.0001$) because of the primary production from macrophytes peaks in summer in the two clear water ponds.

The correlations between pCO_2 and precipitation, and between dissolved CH_4 concentration and water temperature observed in all four ponds individually were also observed and when pooling together the data for all four ponds data were pooled together (Tables S46, S57 "All" in Table S3; Fig S7). The slopes of these correlations were not significantly different between ponds and were not correlated with surface area, depth, or dominance of type of primary producers (phytoplankton or macrophyte) (Table S6). These results suggesting that the effect of precipitation on pCO_2 and the impact of water temperature on dissolved CH_4 concentration outweigh other factors such as pond size and depth in explaining seasonal variations.

The %N₂O values ranged from 32 to 826% (Fig. 3), within the range of values observed in other ponds (Audet et al., 2020; Rabaey and Cotner, 2022). Undersaturation of N₂O with respect to atmospheric equilibrium was observed 66 times out of the 187 measurements. Low values of %N₂O were generally observed in spring and summer and high values of %N₂O were generally observed in fall and winter in the four ponds (Fig. 3). During spring, the %N₂O was lower in the Pêcheres pond (90±11%) than the Leybeek (138±30%, Tukey's HSD test $p=0.0043$, Table S3) and the Tenreuken (138±41, Tukey's HSD test $p=0.0057$, Table S3) ponds. During summer, the %N₂O was lower in the Pêcheres pond (78±17%) than the Leybeek (191±104%, Tukey's HSD test $p<0.0001$, Table S3) and the Silex (126±49%, Tukey's HSD test $p=0.001$, Table S3) pond, and lower in the Tenreuken pond (133±106%) than the Leybeek pond (Tukey's HSD test $p=0.0219$, Table S3). During fall, %N₂O was lower in the Pêcheres pond (103±33%) than the Leybeek pond (190±70%, Tukey's HSD test $p=0.07174$, Table S3). When data were pooled together For the all sampling period, %N₂O was lower in the Pêcheres pond (94±28-%) than the Leybeek (178±82 %, $p<0.0001$, Table S7), Tenreuken (140±77-%, $p<0.0001$, Table S7) and Silex (144±113-%, $p<0.0001$, Table S7) ponds, and was lower in the Tenreuken pond than the Leybeek pond ($p=0.0038$, Table S7). When data were pooled together, %N₂O was correlated negatively ~~correlated to~~ with water temperature and positively ~~correlated to~~ with DIN, more particularly positively correlated to and NH₄⁺ when data were pooled together (Table S4). In individual ponds, %N₂O was negatively correlated to with water temperature in the Leybeek, Pêcheres, and Tenreuken ponds (Table S5). %N₂O was positively correlated with NO₃⁻ in the Leybeek pond and, with NH₄⁺ in the Pêcheres and Tenreuken ponds (Table S8). The %N₂O was positively correlated with Chl-*a* and TSM in the Tenreuken pond, and negatively with Chl-*a* in the Leybeek pond (Table S5), but probably indirectly reflecting the negative correlation of Chl-*a* and TSM with water temperature in this the Tenreuken pond and the positive correlation of Chl-*a* with water temperature in the Leybeek pond (Table S6). The %N₂O values did not show significant seasonal variations in any of the four sampled ponds (ANOVA $F(3,174)=1.127$, $p=0.4091$) (Fig. 3). In individual ponds, %N₂O correlated negatively to with temperature in the Tenreuken pond and Chl-*a* in the Silex pond, and positively to SRP in the Silex pond and TSM concentration in the Tenreuken pond (Table S3; Fig S3, S4). We do not have a clear explanation for these correlations that might be spurious. The correlations with Chl-*a* and TSM were surprising since they were observed in the two clear water ponds and might indirectly reflect seasonal variations (with minimal values of these two quantities in summer). More surprisingly, %N₂O was not correlated with DIN (Table S3; Fig S3, S4, S5, S6) nor with individual forms of DIN (NH₄⁺, NO₂⁻, NO₃⁻) in the four ponds individually or when all the data were pooled together for the individual forms of DIN (Table S3; Fig S7). In a previous study of the variation of GHGs in 22 urban ponds in the city of Brussels sampled only once during each season, %N₂O correlated positively with DIN, NH₄⁺, NO₂⁻, and NO₃⁻. The range of variation of DIN and %N₂O across these 22 ponds (2 to 625 μmol L⁻¹ for DIN, and 0 to 10,354% for %N₂O) was wider than the one observed in the present study of only four ponds (1 to 135 μmol L⁻¹ for DIN, and 32 to 826% for %N₂O) (Fig. S8). The four ponds studied here are located at the periphery of the city and most probably receive less atmospheric nitrogen deposition than closer to the city center. A lower atmospheric nitrogen deposition in the periphery than in the city center is consistent with the correlation between %N₂O and atmospheric nitrogen dioxide (NO₂), and the correlation between %N₂O and the distance from the city center (Fig. S8). Atmospheric nitrogen deposition has been shown to enhance denitrification and N₂O production in lakes (McCrackin and Elser, 2010; Palacin-Lizarbe et al., 2020).

The relationships between GHG dissolved concentrations and other variables were similar in clear water macrophyte-dominated ponds and turbid water phytoplankton-dominated ponds. pCO₂ was positively correlated with precipitation, and dissolved CH₄ concentration was positively correlated with temperature, while no significant correlation was found between %N₂O and other variables in the four ponds taken individually. The negative correlation between pCO₂ and %O₂ reflected the photosynthesis respiration balance independently from the community driving aquatic primary production (macrophytes in clear water ponds and phytoplankton in turbid water ponds).

3.2. Drivers of bubble flux

The bubble flux measured with inverted funnels in the four sampled ponds in the city of Brussels ranged between 0 and 2078 $\text{mL m}^{-2} \text{d}^{-1}$ and ~~strongly was positively correlated with increased with~~ water temperature (Fig. 4) ~~and were overall higher in summer ($837 \pm 434 \text{ mL m}^{-2} \text{d}^{-1}$) than in spring ($198 \pm 170 \text{ mL m}^{-2} \text{d}^{-1}$) and fall ($106 \pm 63 \text{ mL m}^{-2} \text{d}^{-1}$) (Tukey's HSD test $p < 0.0001$ for summer versus spring and summer versus fall).~~ The bubble flux values in the four sampled ponds in the city of Brussels ~~were within the range of values reported in lentic systems of equivalent size by Wik et al. (2013) (0 to $2772 \text{ mL m}^{-2} \text{d}^{-1}$), Delsontro et al. (2016) (11 to $748 \text{ mL m}^{-2} \text{d}^{-1}$) and Ray and Holgerson (2023) (0 to $2079 \text{ mL m}^{-2} \text{d}^{-1}$).~~ The mean CH_4 content of the bubbles in the four sampled ponds in the city of Brussels was $31 \pm 21\%$, ~~and values were positively correlated with water temperature (Fig. 4). The mean values of CH_4 content of the bubbles was correlated with bubble flux (Fig. S3)NEW) as both variables correlated positively with water temperature (Fig. 4).~~ and comparable to the values obtained by Wik et al. (2013) ($35 \pm 25\%$), Delsontro et al. (2016) ($58 \pm 25\%$) and Ray and Holgerson (2023) ($25 \pm 13\%$) in lentic systems of equivalent size. The CH_4 content of the bubbles increased with bubble flux (Fig. 4). These patterns between bubble flux and temperature and $\% \text{CH}_4$ were most probably related to the strong dependence of methanogenesis on temperature (Schulz and Conrad, 1996). The increase of methanogenesis with temperature leads to the build up of gas bubbles in sediments that are richer in CH_4 , and consequently to higher bubble fluxes with a higher CH_4 content at higher temperatures.

~~Bubbling events are known to also be triggered by a decrease of hydrostatic pressure on the sediments due to water level fluctuations or changes in atmospheric pressure. Drops in atmospheric pressure have been documented to trigger bubble fluxes from lake sediments (Tokida et al., 2007; Scandella et al., 2011; Varadharajan and Hemond, 2012; Wik et al., 2013; Taoka et al., 2020; Zhao et al., 2021).~~ The bubble fluxes were measured during more lengthy series at the Silex pond than the other three ponds for logistical reasons allowing investigating ~~in more the detail~~ the effects of water temperature and atmospheric pressure variations on bubble fluxes in more detail. In spring 2022, the bubble flux at the Silex pond increased during events of drops in atmospheric pressure (depressions) (Fig. 5). There was no relation between wind speed and peaks of bubble flux ($r^2 = 0.01$, $p = 0.4629$) ~~as shown in Gatun Lake (Keller and Stallard, 1994), suggesting a more important role of changes of atmospheric pressure than wind speed in the Silex pond in spring 2022.~~ The bubble flux at the Silex pond was higher in summer ($1152 \pm 433 \text{ mL m}^{-2} \text{d}^{-1}$) than during spring ($198 \pm 170 \text{ mL m}^{-2} \text{d}^{-1}$) ~~(Tukey's HSD test $p < 0.0001$), and the temporal changes of bubble fluxes tracked those of water temperature (Fig. 5).~~ The bubble flux was modelled as function of water temperature alone or as function of both water temperature and atmospheric pressure changes (Figs. 5, S49). For periods of low temperature ($< 15^\circ\text{C}$), ~~The the~~ inclusion of the term of air pressure drops in the model of the term of pressure drops in addition to temperature improved the performance of the model ~~compared by to comparison to the measurements (Figs. 5, S49).~~ ~~Bthe original data, for periods of low temperature ($< 15^\circ\text{C}$) but not for warmer periods ($> 15^\circ\text{C}$), when bubbling fluxes were quantitatively more important, the inclusion of the term of air pressure drops in the model did not improve the performance of the model (Figs. 5, S49)(Figs. 5, S9) when bubbling fluxes were quantitatively more important.~~ For the full temperature range ($< 15^\circ\text{C}$ and $> 15^\circ\text{C}$), ~~The the~~ inclusion of the term of air pressure changes drops only improved the performance of the model ~~compared to the original data very marginally (Fig. S4) when comparing the full temperature range ($< 15^\circ\text{C}$ and $> 15^\circ\text{C}$) (Fig. S9), showing that the intensity of bubble flux was mainly driven by temperature change at yearly scales, in agreement with previous studies (e.g. Wik et al., 2013; DelSontro et al., 2016; Aben et al., 2017; Ray and Holgerson, 2023).~~

484 3.3. Drivers of methane ebullitive fluxes

485 Ebullitive CH₄ fluxes in the four ponds ranged between 0 and 59 mmol m⁻² d⁻¹, within the range reported in lentic systems
486 (e.g. Deemer and Holgerson, 2021) and were positively related to water temperature (Fig. 6) as shown previously in other
487 small lentic systems (e.g. Wik et al., 2013; DelSontro et al., 2016; Aben et al., 2017; Ray and Holgerson, 2023; Rabaey and
488 Cotner, 2024). The fitted relations between ebullitive CH₄ fluxes and water temperature were specific to each pond and
489 encompassed the fitted relations established in similar systems: four small ponds in Québec (DelSontro et al., 2016) and a
490 small urban pond in the Netherlands (Aben et al., 2017). The Q₁₀ of CH₄ ebullition values ranged between 4.4 in the deeper
491 Pêcherries pond and 26.9 in the shallower Leybeek pond, respectively (Table S97). The Q₁₀ of CH₄ ebullition in the four
492 studied ponds of the city of Brussels, in Québec (DelSontro et al., 2016), and in the Netherlands (Aben et al., 2017) were
493 negatively related to water depth (Fig. 6). An increase in water temperature leads to a smaller increase in CH₄ ebullitive
494 fluxes (lower Q₁₀) in deeper ponds as the impact of hydrostatic pressure on sediments is higher in deeper ponds compared to
495 shallow ponds, restricting bubble formation and release (e.g. DelSontro et al., 2016).

496 3.4. Relative contribution of methane ebullitive and diffusive fluxes

497 Diffusive CH₄ fluxes computed from dissolved CH₄ concentration and *k* derived from wind speed ranged between 0.1 and
498 19.7 mmol m⁻² d⁻¹ (Fig. 7) within the range reported in lentic systems (e.g. Deemer and Holgerson, 2021). The diffusive CH₄
499 fluxes tended to be higher in summer and spring than in fall and winter owing to the strong positive dependency between
500 CH₄ dissolved concentration and water temperature (Fig. 3; Tables S4, S53). In addition, wind speed only showed small
501 seasonal variations during sampling (0.6±0.6 m s⁻¹ in spring, 0.3±0.2 m s⁻¹ in summer, 0.7±0.7 m s⁻¹ in fall, and 0.6±0.2 m s⁻¹
502 in winter) (Fig. S52). Ebullitive CH₄ fluxes were calculated from the relations with water temperature for each pond given in
503 Figure 6 from the water temperature data coincident with the diffusive CH₄ fluxes (Fig. 7). The resulting calculated
504 ebullitive CH₄ fluxes allowed to compare and integrate seasonally both components of CH₄ emissions to the atmosphere, and
505 to calculate the relative contribution of ebullition to total (diffusive+ebullitive) CH₄ emissions.

506 The relative contribution of ebullition to total CH₄ emissions ranged between 1 and 99% in the four sampled ponds in the
507 city of Brussels (Fig. 7), within the range reported in lentic systems (e.g. Deemer and Holgerson, 2021). Owing to the strong
508 dependency of ebullitive CH₄ fluxes to temperature (Fig. 6; Table S97; Fig. 6), the mean relative contribution of ebullition to
509 total CH₄ emissions for all data pooled together was higher in summer (85±7 %) compared to spring (69±14 %, Tukey's
510 HSD test *p*=0.0104), fall (61±18 %, Tukey's HSD test *p*<0.0001), and winter (53±8 %, Tukey's HSD test *p*<0.0001) were and
511 was positively correlated to water temperature (Fig. S5). (Fig. 7). This finding is consistent with other studies showing that
512 ebullitive CH₄ fluxes can account for more than half of total CH₄ emissions in small and shallow lentic systems (e.g. Wik et
513 al., 2013; Deemer and Holgerson, 2021; Ray and Holgerson, 2023; Rabaey and Cotner, 2024). The relative contribution of
514 ebullition to total CH₄ emissions was lowest during the other seasons, especially in the Leybeek pond (Fig. 7). Owing to the
515 strong dependency of ebullitive CH₄ fluxes to temperature, the relative contribution of ebullition to total CH₄ emissions was
516 related to temperature in the four ponds (Fig. S10), as previously also shown in Québec ponds (DelSontro et al., 2016).

517 The values of Q₁₀ of diffusive CH₄ fluxes were lower than those for ebullitive CH₄ fluxes in each pond, and less variable (1.2
518 in the Pêcherries pond to 2.9 in the Silex pond), and less statistically significant (Table S97). Other studies have also reported
519 higher Q₁₀ for CH₄ ebullition than for CH₄ diffusion in lentic systems (DelSontro et al., 2016; Xun et al., 2024). Higher Q₁₀
520 values for ebullitive CH₄ fluxes than for diffusive CH₄ fluxes lead to an increase in the relative contribution of ebullition to
521 total CH₄ emissions with increasing temperature in the four ponds. The lower dependence to temperature of CH₄ diffusion
522 compared to CH₄ ebullition might be related to a lower relative change of CH₄ concentrations and *k* to temperature change.

CH₄ concentrations in surface water are very strongly affected by MOX (see hereafter). A relative increase of CH₄ production in sediments by methanogenesis will lead to a stronger increase of CH₄ emission by ebullition than by diffusion because of a mitigation by MOX on CH₄ diffusion. Additionally, k depends on wind speed, but the warmer periods of the year (summer) tended to be less windy ($\sim 0.3 \text{ m s}^{-1}$) than the other seasons ($> 0.6 \text{ m s}^{-1}$) also contributing to lower dependence on temperature of CH₄ diffusion compared to ebullition and lower Q_{10} values.

The annually averaged diffusive and ebullitive fluxes of CH₄ in the four ponds in the city of Brussels were plotted against annually averaged Chl-*a* concentration, total macrophyte cover in summer, water depth, and lake surface area (Fig. 8) that are frequent predictors of variations of CH₄ fluxes among lakes (Holgerson and Raymond, 2016; DelSontro et al., 2018, Deemer and Holgerson, 2021; Casas-Ruiz et al., 2021; Borges et al., 2022). The annually averaged diffusive CH₄ flux was significantly lower in the slightly deeper Pêcheries pond (130 cm depth) than the two slightly shallower ponds (Leybeek (60 cm depth) and Silex (110 cm depth) ponds) (Tukey's HSD test $p=0.0007$ for Pêcheries versus Leybeek, $p<0.0001$ for Pêcheries versus Silex), and the annually averaged ebullitive CH₄ flux was significantly lower in the Pêcheries pond than the Silex pond (Tukey's HSD test $p<0.0001$) but was not significantly different than the Leybeek pond (Tukey's HSD test $p=0.3847$). No other significant differences in annually averaged diffusive and ebullitive CH₄ fluxes related to water depth or surface area were observed. The narrow range of variation of water depth (50 to 150 cm) and surface area (0.7 to 3.2 ha) could explain the lack of a clear decrease of diffusive and ebullitive CH₄ fluxes with increasing depth or surface that are frequent predictors of variations of CH₄ fluxes among ponds (e.g. Holgerson, 2015; Holgerson and Raymond, 2016; Ray et al., 2023; Theus et al., 2023) and lakes (e.g. Kankaala et al., 2013; DelSontro et al., 2018; Deemer and Holgerson, 2021; Casas-Ruiz et al., 2021; Borges et al., 2022). Correlations between CH₄ fluxes and depth or lake surface area have been shown among lakes across much larger ranges of variation of lake depth (Borges et al., 2022) and surface area (Kankaala et al., 2013; Holgerson and Raymond, 2016; Casas-Ruiz et al., 2021).

The annually averaged ebullitive CH₄ fluxes were significantly higher in the two clear-water ponds (7.3 ± 2.9 and $13.4 \pm 3.7 \text{ mmol m}^{-2} \text{ d}^{-1}$ in the Tenreuken and Silex ponds, respectively) than the two turbid-water ponds (3.8 ± 3.2 and $2.5 \pm 1.4 \text{ mmol m}^{-2} \text{ d}^{-1}$ in the Leybeek and Pêcheries ponds, respectively) (Tukey's HSD test $p<0.0001$ for each comparison between a clear-water pond and a turbid-water pond Table S7). The annually averaged ebullitive CH₄ fluxes were significantly higher in the Silex pond, that showed a higher macrophyte cover during summer (100% in the Silex pond and 68% in the Tenreuken pond), than the Tenreuken pond (Tukey's HSD test $p<0.0001$, Table S7) that showed a higher macrophyte cover during summer (100% in the Silex pond and 68% in the Tenreuken pond) and were not significantly different in the two turbid-water Leybeek and Pêcheries ponds (Tukey's HSD test $p=0.0617$, Table S7 3847) that showed similar macrophyte cover during summer (6 and 9% in the Leybeek and Pêcheries ponds, respectively) (Fig. 8). The annually averaged ebullitive CH₄ fluxes were overall positively correlated to with macrophyte cover and negatively correlated to with Chl-*a* (Fig. 8). The higher ebullitive CH₄ emissions from the clear-water ponds would suggest that the delivery of organic matter to sediments from macrophytes sustained a larger methane production than from phytoplankton. This finding is consistent with the notion that vegetated littoral zones of lakes are hot spots of CH₄ production and emission (e.g. Hyvönen et al., 1998; Huttunen et al., 2003; Juutinen et al., 2003; Desrosiers et al., 2022). In other small lentic systems, the CH₄ dissolved concentrations and diffusive fluxes have also been shown to correlate positively with macrophyte cover (e.g. Ray et al., 2023; Theus et al., 2023).

The annually averaged diffusive CH₄ flux was higher in the two clear-water ponds (1.4 ± 0.7 and $1.9 \pm 0.4 \text{ mmol m}^{-2} \text{ d}^{-1}$ in the Tenreuken and Silex ponds, respectively) than in the turbid-water Pêcheries pond ($1.0 \pm 0.3 \text{ mmol m}^{-2} \text{ d}^{-1}$) (Tukey's HSD test

$p=0.0404$ for Tenreken versus Pêcherries, and $p<0.0001$ for Silex versus Pêcherries), which was consistent with the pattern of higher ebullitive CH_4 emissions from clear-water ponds (Fig. 8). In the four sampled urban ponds, annually averaged CH_4 diffusive fluxes were significantly higher in the pond with the highest total macrophyte cover in the clear-water ponds, and significantly higher in the pond with the highest Chl-*a* concentration in the turbid-water ponds (Fig. 8). An increase in methane production with phytoplankton biomass in turbid-water ponds has also been reported by other studies in lakes (e.g. Yan et al., 2019; Bartosiewicz et al., 2021). Since total macrophyte cover and Chl-*a* were anti-correlated, we hypothesize that the variations of CH_4 diffusive fluxes follow a U-shaped relation with either Chl-*a* or macrophyte cover. Higher values of annual CH_4 diffusive fluxes occurred at the extreme values of Chl-*a* or of macrophyte cover (minimum or maximum), and lower values occurred at the intermediate values of Chl-*a* or macrophyte cover. The annually averaged relative contribution of ebullition to total CH_4 emissions were higher in the two clear-water ponds than the two turbid-water ponds (Table S7). The relative contribution of ebullitive CH_4 fluxes to the total flux was higher in the clear-water Silex pond, which had the highest macrophyte cover, compared to the two turbid-water ponds with lower macrophyte cover (Tukey's HSD test $p<0.0001$ for Silex versus Leybeek, $p=0.0056$ for Silex versus Pêcherries), and was higher in the clear-water Tenreken pond than in the turbid-water Leybeek pond (Tukey's HSD test $p<0.0001$) (Fig. 8). The relative contribution of ebullitive CH_4 fluxes to the total CH_4 flux seems to increase concomitantly with the macrophyte cover (Fig. 8), and was overall strongly positively correlated to with macrophyte cover and negatively to Chl-*a* (Fig. 8). These patterns are consistent with the idea of an increase of ebullition relative to diffusive CH_4 emissions in vegetated sediments compared to unvegetated sediments (e.g. Desrosiers et al., 2022; Ray et al., 2023; Theus et al., 2023).

The annual diffusive and ebullitive fluxes in the four ponds in the city of Brussels were within the range of values for ponds of similar surface area (0.4 to 4.0 ha) compiled by Deemer and Holgerson (2021) (Fig. S11). The linear regression of ebullitive CH_4 fluxes as a function of diffusive CH_4 fluxes allows comparing the data of ebullitive CH_4 fluxes from the four Brussels ponds "normalized" to the diffusive CH_4 fluxes. The ebullitive CH_4 fluxes from the two turbid-water ponds (Pêcherries and Leybeek) were very close to the linear regression showing they were characterized by ebullitive CH_4 fluxes equivalent to those in the ponds compiled by Deemer and Holgerson (2021) when normalized by the diffusive fluxes. The ebullitive CH_4 fluxes from the two clear-water ponds (Tenreken and Silex) were above the linear regression showing they were characterized by ebullitive CH_4 fluxes above those in the ponds compiled by Deemer and Holgerson (2021) when normalized by the diffusive fluxes. We hypothesize the relatively higher ebullitive fluxes in the two clear-water ponds were related to enhancement of ebullition from organic matter subsidized by macrophytes. This hypothesis is consistent with the two clear-water ponds in Brussels having higher ebullitive fluxes than in the ponds compiled by Deemer and Holgerson (2021) at equivalent Chl-*a* values (Fig. S11). The observed high ebullitive fluxes in the clear-water ponds would suggest that Chl-*a* concentration alone fails to predict ebullitive fluxes in macrophyte-dominated clear-water ponds. Consequently, global scaling of CH_4 fluxes in lentic systems using Chl-*a* as a predictor as used in lakes (e.g. DelSontro et al., 2018) might underestimate ebullitive CH_4 emissions due to a misrepresentation of macrophyte-dominated clear-water ponds.

The annually averaged diffusive fluxes of CO_2 (F_{CO_2}) and N_2O ($F_{\text{N}_2\text{O}}$) in the four ponds in the city of Brussels were also plotted against annually averaged Chl-*a* concentration, total macrophyte cover in summer, water depth, and lake surface area, as well as DIN for N_2O fluxes (Fig.s. S612, S13, S14). Annually averaged F_{CO_2} were lower in the Leybeek pond than the Pêcherries and Silex ponds (Table S7). did not show significant differences between the four studied ponds (Tukey's HSD test: $p>0.05$ for each comparison), and F_{CO_2} did not significantly correlate to with the other variables (Chl-*a* concentration, total macrophyte cover, water depth, and lake surface area). This might be surprising since other studies have reported lower CO_2 fluxes in more productive lentic systems (e.g. Sand-Jensen and Staehr 2007; Borges et al. 2022). We hypothesize that

given that the four systems were either phytoplankton-dominated or macrophyte-dominated, in both cases, the ponds had an important submerged productivity resulting in a relatively invariant F_{CO_2} as function of either Chl *a* or macrophyte cover. Annually averaged mean F_{CO_2} was also uncorrelated to water depth and lake area (Fig. S612). This might have resulted from the relative similarity of depth and surface area of the four studied ponds, as it is well established that CO_2 emissions strongly increase with decreasing size of ponds (Holgerson and Raymond, 2016). Annual F_{N_2O} was not significantly different between clear-water and turbid-water ponds. F_{N_2O} was significantly lower in the slightly deeper Pêcheries pond than the two slightly shallower Leybeek and Silex ponds (Fig. S6, Table S713) (Tukey's HSD test $p=0.0012$ for Pêcheries vs. Leybeek, and $p=0.0052$ for Pêcheries vs. Silex), and F_{N_2O} showed a significant negative relationship with water depth (Fig. S613). We hypothesize that this might reflect a larger dilution of N_2O diffusing from sediments in the deeper systems. F_{N_2O} did not correlate to DIN, NH_4^+ , NO_2^- , and NO_3^- (Fig. S14). We hypothesize that this reflects the rather narrow range of annual DIN average values in the four studied ponds (~ 24 to $\sim 29 \mu mol L^{-1}$), as DIN, NH_4^+ , NO_2^- , and NO_3^- were not statistically different between ponds (Tukey's HSD test $p>0.05$ for every comparison).

3.5. Methanogenesis pathway inferred from $\delta^{13}C-CH_4$ in bubbles

$\delta^{13}C-CH_4$ was measured in bubbles trapped during the ebullition flux measurements and in bubbles collected by perturbing the sediments. The variations of $\delta^{13}C-CH_4$ suggest that there could have been variations of the relative importance of hydrogenotrophic versus acetoclastic pathways of methanogenesis among different ponds but also seasonally. Methanogenesis by the hydrogenotrophic pathway produces CH_4 with more negative $\delta^{13}C-CH_4$ values (-100‰ to -60‰) compared to the acetoclastic pathway (-65‰ to -50‰) (Whiticar et al., 1986). Yet, it remains unclear which environmental factors determine the relative importance of hydrogenotrophic and acetoclastic methanogenesis pathways (Conrad et al., 2011).

The $\delta^{13}C-CH_4$ values in the trapped bubbles for the all dataset were statistically more negative in fall ($-83.2 \pm 5.2 \text{‰}$) than summer ($-69.5 \pm 3.2 \text{‰}$) and spring ($-68.2 \pm 4.4 \text{‰}$) (Fig. 9; Table S8) (Tukey's HSD test $p<0.0001$ for fall versus summer, and fall versus spring), suggesting a dominance of hydrogenotrophic methanogenesis in fall compared to spring and summer when acetoclastic methanogenesis seemed dominant. Hydrogenotrophic methanogenesis occurs at higher temperatures than acetoclastic methanogenesis (Schulz and Conrad, 1996; Schulz et al., 1997), however, temperature in fall ($11.9 \pm 3.7 \text{ °C}$) was lower than in summer ($21.1 \pm 1.9 \text{ °C}$) (Tukey's HSD test $p<0.0001$). A shift from acetoclastic methanogenesis to hydrogenotrophic methanogenesis has been documented in response to the increase of NH_4^+ concentration (Ni et al., 2022; Wang et al., 2022) and the decrease of pH (Kotsyurbenko et al., 2007) expected in response to an increase of CO_2 . An increase of NH_4^+ and decrease of pH in pore waters in fall compared to summer and spring would be consistent with the sustained benthic organic matter degradation leading to a gradual change of pore water chemistry from spring to fall.

In summer 2023, a survey of all four ponds was made to simultaneously sample bubbles by perturbation of the sediment for the determination of the $\delta^{13}C-CH_4$ in the released bubbles. The $\delta^{13}C-CH_4$ values of perturbed sediments were more negative in the clear-water macrophyte-dominated ponds ($-80.1 \pm 0.1 \text{‰}$ and $-78.4 \pm 1.2 \text{‰}$ in the Tenreuken and Silex ponds, respectively) than in the turbid-water phytoplankton-dominated ponds ($-69.7 \pm 0.7 \text{‰}$ and $-70.7 \pm 0.4 \text{‰}$ in the Leybeek and Pêcheries ponds, respectively) (Tukey's HSD test $p<0.0001$ for each comparison between a clear pond and a turbid pond) (Fig. 10). This pattern of $\delta^{13}C-CH_4$ of perturbed sediments could suggest a higher contribution of the hydrogenotrophic methanogenesis pathway compared to the acetoclastic pathway in the clear-water ponds where organic matter for methanogenesis was assumed to be mainly related to macrophytes rather than phytoplankton. Based on gene expression during incubations, Wang et al. (2023) suggested that acetoclastic methanogenesis pathway was stimulated by macrophyte

organic carbon compared to phytoplankton organic matter in lakes Chaohu and Taihu in China. The distribution of $\delta^{13}\text{C}-\text{CH}_4$ data in the four urban ponds of the city of Brussels suggests the opposite pattern, with macrophyte organic carbon stimulating the hydrogenotrophic methanogenesis pathway. This pattern seems consistent with the more refractory nature of macrophyte organic carbon compared to the more labile nature of phytoplankton organic carbon. Organic matter from macrophytes has a large share of molecules difficult to degrade such as cellulose unlike organic matter from phytoplankton that is rich in polysaccharides and proteins (West et al., 2015; Berberich et al., 2020). In presence of more refractory organic matter, a partial fermentation would favour the production of H_2 over acetate which would favour hydrogenotrophic methanogenesis over acetoclastic methanogenesis (Liu et al., 2017).

3.6. Methane oxidation

The $\delta^{13}\text{C}-\text{CH}_4$ of dissolved CH_4 in surface waters in the four sampled ponds in the city of Brussels ranged between -16 and -64 ‰ (Fig. 11). The $\delta^{13}\text{C}-\text{CH}_4$ of dissolved CH_4 in surface waters were generally higher than in sediments based on trapped bubbles during the ebullition measurements (-55 to -87 ‰; Fig. 9). The ^{13}C -enriched values of dissolved CH_4 in surface waters samples probably resulted from MOX. FOX in surface waters in the four sampled ponds in the city of Brussels ranged between 22 and 97%. MOX in surface waters in the four sampled ponds in the city of Brussels ranged between 0.1 and 73.0 $\text{mmol}\cdot\text{m}^{-2}\cdot\text{d}^{-1}$ (Fig. 11).

FOX and MOX followed the same seasonal variations as $\delta^{13}\text{C}-\text{CH}_4$ of dissolved CH_4 since both quantities were derived from isotopic models that include $\delta^{13}\text{C}-\text{CH}_4$ of dissolved CH_4 . $\delta^{13}\text{C}-\text{CH}_4$ of dissolved CH_4 , FOX, and MOX showed no significant differences between seasons in the two turbid-water ponds except in the Pêcheries pond where MOX was lower in winter ($1.3\pm0.86\text{ mmol}\cdot\text{m}^{-2}\cdot\text{d}^{-1}$) than in summer ($12.3\pm10.5\text{ mmol}\cdot\text{m}^{-2}\cdot\text{d}^{-1}$, Tukey's HSD test $p=0.0010$) and fall ($6.5\pm3.0\text{ mmol}\cdot\text{m}^{-2}\cdot\text{d}^{-1}$, Tukey's HSD test $p=0.0254$) (Fig. 11). In the clear-water Silex pond, FOX was lower in spring ($42\pm12\%$) and summer ($52\pm16\%$) than in fall ($84\pm9\%$) and winter ($76\pm12\%$) (Tukey's HSD test $p<0.0001$ for spring or summer versus fall or winter). In the clear-water Tenreuken pond, FOX was higher in fall ($73\pm5\%$) than in spring ($42\pm17\%$, Tukey's HSD test $p<0.0001$) and summer ($57\pm11\%$, Tukey's HSD test $p=0.0324$), and higher in winter ($71\pm10\%$) than in spring ($42\pm17\%$, Tukey's HSD test $p<0.0001$). $\delta^{13}\text{C}-\text{CH}_4$ of dissolved CH_4 and FOX were statistically higher in the turbid-water ponds (Leybeek and Pêcheries) than in the clear-water ponds (Tenreuken and Silex) during spring and summer (Fig. 11) and than in the Tenreuken pond during fall and winter (Fig. 11; Tables S4 and S5). These seasonal differences led to an annual MOX that was statistically higher in the turbid-water ponds (10.8 and 7.2 $\text{mmol}\cdot\text{m}^{-2}\cdot\text{d}^{-1}$ in the Leybeek and Pêcheries ponds, respectively) than the clear-water ponds (2.4 and 4.4 $\text{mmol}\cdot\text{m}^{-2}\cdot\text{d}^{-1}$ in the Tenreuken and Silex ponds, respectively) (Tukey's HSD test $p<0.0001$ for each turbid-water pond versus each clear-water pond). TSM and Chl *a* concentrations were higher in the turbid-water ponds than in the clear-water ponds, particularly during productive phytoplanktonic periods of spring and summer (Fig. 3), when the highest difference of $\delta^{13}\text{C}-\text{CH}_4$ of dissolved CH_4 , FOX, and MOX were observed between the turbid-water and the clear-water ponds (Fig. 11).

$\delta^{13}\text{C}-\text{CH}_4$ of dissolved CH_4 , FOX, and MOX positively correlated to TSM and Chl *a* concentrations (Fig. 12). These patterns could reflect the increase of micro-organisms including methanotrophs fixed on particles leading to an increase of MOX in parallel to an increase of TSM concentration (Abril et al., 2007). Fixed micro-organisms can grow on inorganic particles and aggregates of organic matter (Kirchman and Mitchell, 1982), but also on aggregates of living cyanobacteria (Li et al., 2021). An increase of particles in the water column increases light attenuation in the water column which would alleviate the inhibition of MOX by light (Dumestre et al., 1999; Murase and Sugimoto 2005; Morana et al., 2020), also possibly

contributing to a positive relation between MOX and TSM and Chl α , along the turbidity gradient. Both processes could occur contributing to the observed positive patterns between MOX and TSM and Chl α concentrations.

Figure S15 compares the main fluxes of dissolved CH₄ in the water column: MOX, diffusive CH₄ emissions, bubble dissolution that were derived from measurements, and the sedimentary diffusive CH₄ flux that was computed as a closing term (assuming a steady state) for comparative purposes. The dissolution of bubbles was a significantly smaller input term of dissolved CH₄ compared to the diffusive sedimentary flux that represented 88±18 % of the total input of CH₄ to the water column (Tukey's HSD test $p < 0.0001$ in each pond). The low contribution of dissolution of bubbles resulted from the shallowness of the studied ponds because bubble dissolution depends on the time spent by the bubble in the water column during ascent, which is directly proportional to depth (McGinnis et al., 2006). MOX was a larger sink of dissolved CH₄ than the diffusive CH₄ emission to the atmosphere in the four ponds, representing 80±19 % and 80±14 % of the total dissolved CH₄ removal in the turbid water Leybeek and Pêcherries ponds respectively (Tukey's HSD test $p < 0.0001$ for the two ponds), and 59±21 % and 51±27 % in the clear water Tenreuken and Silex ponds respectively (Tukey's HSD test $p = 0.3429$ for the Tenreuken pond, and $p = 0.7634$ for the Silex pond). For all four ponds, MOX accounted for 66±26 % of the total CH₄ dissolved removal from the water column, in agreement with other studies in lentic systems (Kankaala et al., 2006; Bastviken et al., 2008; Morana et al., 2020; Reis et al., 2022).

3.7.3.5. Relative contribution of CO₂, CH₄ and N₂O emissions

The emissions in CO₂-eq for the 3 GHGs averaged per season for both 2022 and 2023 peaked seasonally in summer with 2.9 and 1.7 mg CO₂-eq m⁻² d⁻¹ in the Silex and the Tenreuken ponds, respectively, and 1.1 mg CO₂-eq m⁻² d⁻¹ in the Leybeek pond (Fig. 913). The GHG fluxes in CO₂-eq peaked in fall in the Pêcherries pond, with 1.3 mg CO₂-eq m⁻² d⁻¹. The higher value of the total GHG emissions in fall compared to other seasons in the Pêcherries pond was due to an increase of CO₂ emissions in fall that surpassed the peak of CH₄ emissions in summer. The GHG fluxes were the lowest in winter with 1.3 and 0.9 mg CO₂-eq m⁻² d⁻¹ in the Silex and the Tenreuken ponds, respectively, and 0.8 and 0.6 mg CO₂-eq m⁻² d⁻¹ in the Pêcherries and the Leybeek ponds, respectively. The relative contribution of ebullitive CH₄ fluxes peaked in summer in all four ponds, 73.8% and 70.9% in the Silex and the Tenreuken ponds, respectively, and 23.6% and 58.3% in the Pêcherries and the Leybeek ponds, respectively. The relative contribution of ebullitive CH₄ fluxes was the lowest in winter with 22.1% and 10.0% in the Silex and the Tenreuken ponds, respectively, and 6.7% and 1.0% in the Pêcherries and the Leybeek ponds, respectively.

The annual emissions in CO₂-eq of the three GHGs (CO₂, CH₄, and N₂O) in 2022 and 2023 were higher in the two clear-water ponds (1.3±0.5 and 1.8±0.9 mg CO₂-eq m⁻² d⁻¹ in the Tenreuken and Silex ponds, respectively) than in the two turbid-water ponds (1.0±0.2 and 0.9±0.5 mg CO₂-eq m⁻² d⁻¹ in the Leybeek and Pêcherries ponds, respectively) (Fig. 913) (Tukey's HSD test $p < 0.0001$ for Silex versus Pêcherries, $p < 0.0001$ for Silex versus Leybeek, $p = 0.0107$ for Tenreuken versus Pêcherries, and $p = 0.0467$ for Tenreuken versus Leybeek) due to higher total CH₄ emissions (diffusive+ebullitive) in clear-water ponds (0.7±0.4 and 1.2±0.5 mg CO₂-eq m⁻² d⁻¹ in the Tenreuken and Silex ponds, respectively) than in turbid-water ponds (0.2±0.2 and 0.4±0.3 mg CO₂-eq m⁻² d⁻¹ in the Leybeek and Pêcherries ponds, respectively) (Tukey's HSD test $p < 0.0001$ for Silex versus Pêcherries, $p < 0.0001$ for Silex versus Leybeek, $p = 0.0005$ for Tenreuken versus Pêcherries, and $p = 0.0164$ for Tenreuken versus Leybeek), as there were no significant differences between the four ponds for CO₂ emissions in 2022 and 2023 (Tukey's HSD test $p > 0.05$ for each comparison). CO₂ emissions N₂O emissions were significantly lower in the Pêcherries pond than the Leybeek and Silex ponds (Tukey's HSD test $p = 0.0012$ for Pêcherries versus Leybeek, and $p = 0.0052$ for Pêcherries versus Silex). The contribution of N₂O to the total GHG emissions was marginal and did not affect

the differences in total GHG fluxes between ponds, with the highest contribution observed in the Leybeek pond, with a contribution of 1.7%.

The majority of GHG emissions in CO₂-eq was related to CO₂ and CH₄ (diffusive+ebullitive) in the four ponds. In turbid-water ponds CO₂ represented the largest fraction of GHG emissions (68.5% (2022) and 79.3% (2023) in the Pêcherries pond, and 49.0% (2022) and 58.3% (2023) in the Leybeek pond). In clear-water ponds CH₄ represented the largest fraction of GHG emissions (66.5% (2022) and 63.3% (2023) in the Silex pond, and 60.8% (2022) and 50.0% (2023) in the Tenreuken pond). The higher annual GHG emissions in CO₂-eq from the two clear-water ponds than the turbid-water ponds were related to the higher contribution of ebullitive CH₄ fluxes.

The annual GHG fluxes increased from 2022 to 2023 due to an increase in relative contribution of CO₂ diffusive emissions in all four ponds. Diffusive CO₂ emissions averaged annually in all four ponds 0.5 mg CO₂ m⁻² d⁻¹ in 2022 and 0.7 mg CO₂ m⁻² d⁻¹ in 2023. Diffusive CO₂ emissions were ~~two-2.1~~ times higher in summer 2023 than in summer 2022, and 2.5 times higher in fall 2023 than in fall 2022, ~~for and showed~~ similar values between 2023 and 2022 in spring and winter (1.1 higher and 1.1 lower, respectively). ~~Air temperatures were similar in both years (annual average of 12.2°C in 2022 and 12.1°C in 2023) with winter, spring and summer marginally colder in 2023 than in 2022 (-0.5, -1.1°C and -0.4°C, respectively), and fall marginally warmer in 2023 than 2022 (+0.6°C). Spring, and summer and fall were rainier in 2023 than 2022 (2.2, and 2.5 and 1.5 times, respectively) but fall and winter precipitations were relatively similar in both years (1.4 times wetter and 1.2 times drier in 2023 than 2022, respectively). Higher precipitations are likely to increase the inputs of organic and inorganic carbon from soils to ponds by ground waters, soil waters, and surface runoff, as previously shown in other lentic systems (e.g. Marotta et al., 2011; Holgerson, 2015). The highest seasonal increase of diffusive CO₂ emissions was observed in fall 2023. While this hypothesis is only based on the comparison of two years, the increase of the relative contribution of CO₂ diffusive emissions was observed in all four ponds which suggests a common uniform driver that would be consistent with a large variation weather such as annual precipitation. The El Niño event in 2023 induced low level cyclonic wind anomalies and higher precipitation over Western Europe, including Belgium (Chen et al., 2024).~~

4. Discussion

The Leybeek and Pêcherries ponds are turbid-water systems (high Chl-*a* and TSM values, low submerged macrophyte cover) and the Tenreuken and Silex ponds are clear-water systems (low Chl-*a* and TSM values, high submerged macrophyte cover) (Figs. 1, 3). All four ponds have a relatively similar size (0.7 to 3.2 ha) and depth (0.5 to 1.45 m) and are uniformly located in an urban landscape in the city of Brussels. It can be assumed that, among the four systems, the major difference that is expected to affect GHG emissions is the dominance of aquatic primary producer, either phytoplankton or macrophytes, corresponding to two alternative states *sensu* Scheffer et al. (1993). Our data-set provides the opportunity to test the effect of the two alternative states on GHG emissions from small lentic systems.

The reported pCO₂ values (40 to 13,804 ppm) (Fig. 3) in the four ponds in the city of Brussels were within the range of values typically observed in ponds (Holgerson and Raymond, 2016; Peacock et al., 2019; Audet et al., 2020) (Fig. 3). The pCO₂ values were correlated negatively with %O₂ and positively with DIN and SRP across seasons (ref Fig or Table Tables S4, S5) showing that their seasonal variability was driven by aquatic primary production and degradation of organic matter (e.g. Holgerson 2015). Low values of pCO₂ were generally observed in spring and summer probably due to uptake of CO₂ by primary production from either phytoplankton or submerged macrophytes. High values of pCO₂ were observed in fall in the four ponds and probably reflect the release of CO₂ from degradation of organic matter due to the senescence of

phytoplankton or macrophytes (Fig. 3). In all four ponds, $p\text{CO}_2$ values were positively correlated with precipitation (Tables S3; Figs S3, S4, S5, S46, S5) suggesting an additional control of external inputs of carbon either as organic carbon sustaining internal degradation of organic matter or as soil CO_2 (e.g. Marotta et al., 2010; Ojala et al., 2011; Rasilo et al., 2012; Vachon and del Giorgio, 2014; Holgerson, 2015). The $\%\text{N}_2\text{O}$ values (32 to 826%) (Fig. 3) in the four ponds were within the range typically observed in ponds (Audet et al., 2020; Rabaey and Cotner, 2022). ~~$\%\text{N}_2\text{O}$ did not correlate with any other variable in individual ponds.~~ When pooled all the data together, $\%\text{N}_2\text{O}$ was positively correlated with DIN (Table S4) as frequently reported by other studies in ponds and interpreted as a control of nitrification and/or denitrification (hence N_2O production) by DIN levels (Audet et al., 2020; Webb et al., 2021; Wang et al., 2021; Xie et al., 2024). The negative correlation between $\%\text{N}_2\text{O}$ with temperature (Table S4) might reflect both the effect of the inhibition at low temperatures of the final denitrification step of denitrification leading to an accumulation of N_2O at low temperatures (Velthuis and Veraart, 2022) and but could also indirectly result from the higher DIN values at low temperatures (Table S6) that favor N_2O production. The CH_4 dissolved concentrations (194 to 48,380 nmol L^{-1}) (Fig. 3) in the four ponds were within the range of values typically observed in ponds (Natchimuthu et al., 2014; Holgerson and Raymond, 2016; Peacock et al., 2019; Audet et al., 2020; Rabaey and Cotner, 2022; Ray et al., 2023), and were positively correlated with water temperature in all four ponds and when pooled all the data together (Tables S3; Figs S3, S4, S5, S64, S5), most probably reflecting the increase of sedimentary methanogenesis with temperature (Schulz and Conrad, 1996).

Temperature also exerted a strong control on bubble flux from sediments and ebullitive CH_4 emissions. The bubble flux values (0 and 2078 $\text{ml m}^{-2} \text{d}^{-1}$) in the four sampled ponds (Fig. 4) were within the range of values reported in lentic systems of equivalent size by Wik et al. (2013) (0 to 2772 $\text{mL m}^{-2} \text{d}^{-1}$), DelSontro et al. (2016) (11 to 748 $\text{mL m}^{-2} \text{d}^{-1}$), and Ray and Holgerson (2023) (0 to 2079 $\text{mL m}^{-2} \text{d}^{-1}$). The bubble flux was positively correlated with water temperature (Fig. 4) in agreement with previous studies (e.g. Wik et al., 2013; DelSontro et al., 2016; Aben et al., 2017; Ray and Holgerson, 2023). Bubbling events from lake sediments are known to also be triggered by a decrease of hydrostatic pressure on the sediments due to water level fluctuations or drops in atmospheric pressure (Tokida et al., 2007; Scandella et al., 2011; Varadharajan and Hemond, 2012; Wik et al., 2013; Taoka et al., 2020; Zhao et al., 2021). In the Silex pond, in spring 2022, some peaks in bubble fluxes were related to drops in atmospheric pressure (Fig. 5) but unrelated to wind speed ($r^2 = 0.01$, $p = 0.4629$) as shown in Gatun Lake (Keller and Stallard, 1994). A statistical model of the bubble flux that included the contributions of water temperature and air pressure drops was used to quantify the relative importance of each of these two drivers (Fig. S49). The contribution of the air pressure drop seemed quantitatively important only at low water temperature ($<15^\circ\text{C}$) and was negligible at higher water temperature ($>15^\circ\text{C}$) (Fig. S49). The inclusion of the term of air pressure drops only improved the performance of the model compared to the original data very marginally when comparing across the full water temperature range ($<15^\circ\text{C}$ and $>15^\circ\text{C}$) (Fig. S49), showing that the intensity of bubble flux was mainly driven by temperature change at yearly scales, in agreement with previous studies (e.g. Wik et al., 2013; DelSontro et al., 2016; Aben et al., 2017; Ray and Holgerson, 2023).

The mean CH_4 content of the bubbles ($31 \pm 21\%$) in the four sampled ponds in the city of Brussels was comparable to the values obtained by Wik et al. (2013) ($35 \pm 25\%$), DelSontro et al. (2016) ($58 \pm 25\%$), and Ray and Holgerson (2023) ($25 \pm 13\%$) in lentic systems of equivalent size. The increasing pattern of the CH_4 content of the bubbles with water temperature (Fig. 4X) was most probably related to the strong dependence of methanogenesis on temperature (Schulz and Conrad, 1996). The increase of methanogenesis with temperature leads to the build-up of gas bubbles in sediments that are richer in CH_4 , and consequently to higher bubble fluxes with a higher CH_4 content at higher temperatures (Figs. 4X, SX3). Since both bubble flux and the CH_4 content of the bubbles increased with water temperature (Fig. 4X), the ebullitive CH_4

fluxes in the four ponds were also positively related to water temperature (Fig. 6) as shown previously in other small lentic systems (e.g. Wik et al., 2013; DelSontro et al., 2016; Natchimuthu et al., 2016; Aben et al., 2017; Ray and Holgerson, 2023; Rabaey and Cotner, 2024). Yet, the dependency of CH₄ ebullition on temperature (Q_{10}) was different among the four ponds and was negatively related to depth including data from systems in Québec (DelSontro et al., 2016) and the Netherlands (Aben et al., 2017) (Fig. 6). This implies that an increase in water temperature leads to a smaller increase in CH₄ ebullitive fluxes (lower Q_{10}) in deeper ponds as the impact of hydrostatic pressure on sediments is higher in deeper ponds compared to shallow ponds, restricting bubble formation and release (e.g. DelSontro et al., 2016). This dependence of Q_{10} of CH₄ ebullition to depth suggests that the response of CH₄ ebullition to heatwaves (or longer-term warming) might be more intense the shallower the pond, in addition to other effects from heat-waves on GHG emissions (e.g. Audet et al., 2017).

The values of Q_{10} for diffusive CH₄ fluxes in the four ponds were lower than those for ebullitive CH₄ fluxes (Table S97) as reported by other studies in lentic systems (DelSontro et al., 2016; Xun et al., 2024). The lower dependence to water temperature of diffusive CH₄ fluxes compared to ebullitive CH₄ fluxes might be related to a lower relative change of CH₄ concentrations and k with the variation of water temperature. CH₄ concentrations in surface waters of lentic systems are strongly affected by microbial methane oxidation (e.g. Bastviken et al., 2002). A relative increase of CH₄ production in sediments by methanogenesis might lead to a stronger increase of CH₄ emission by ebullition than by diffusion because of a mitigation by methane oxidation on CH₄ diffusive fluxes. Additionally, k depends on wind speed, but in the four ponds, the warmer periods of the year (summer) tended to be less windy ($\sim 0.3 \text{ m s}^{-1}$) than the other seasons ($> 0.6 \text{ m s}^{-1}$) also contributing to a lower dependence on water temperature of CH₄ diffusive fluxes compared to ebullitive fluxes and lower Q_{10} values.

The difference in the Q_{10} of diffusive and ebullitive CH₄ fluxes was consistent with a variable contribution of the diffusive and ebullitive CH₄ fluxes seasonally as a function of water temperature, with the contribution of ebullitive CH₄ fluxes strongly increasing with water temperature in the four ponds (Fig. S5). At annual scale, ebullitive CH₄ fluxes represented between 55% and 83% of the total CH₄ emissions in the Leybeek and Silex ponds, respectively. This finding is consistent with other studies showing that ebullitive CH₄ fluxes can account for more than half of total CH₄ emissions in small and shallow lentic systems (e.g. Wik et al., 2013; Deemer and Holgerson, 2021; Ray and Holgerson, 2023; Rabaey and Cotner, 2024). The averaged ebullitive CH₄ emissions were higher in the two clear-water ponds ($10.4 \text{ mmol m}^{-2} \text{ d}^{-1}$) than the two turbid-water ponds ($3.2 \text{ mmol m}^{-2} \text{ d}^{-1}$) (Fig 7). The averaged ebullitive CH₄ emissions in the four ponds were positively correlated with macrophyte cover and negatively correlated with Chl-*a* (Fig. 8). The higher ebullitive CH₄ emissions from the two clear-water ponds would suggest that the delivery of organic matter to sediments from macrophytes sustained a quantitatively larger methane production than from phytoplankton. This finding is consistent with the notion that vegetated littoral zones of lakes are hot spots of CH₄ production and emission (e.g. Hyvönen et al., 1998; Huttunen et al., 2003; Juutinen et al., 2003; Desrosiers et al., 2022). CH₄ fluxes in lentic systems have been scaled at globally scale assuming a dependency on aquatic productivity using Chl-*a* as a predictor (e.g. DelSontro et al., 2018). The negative relation between CH₄ ebullitive fluxes with Chl-*a* shows that Chl-*a* concentration alone fails to predict ebullitive fluxes in macrophyte-dominated clear-water ponds.

The annually averaged diffusive CH₄ emissions in the four ponds seemed to respond positively to both increasing phytoplankton and macrophyte biomass resulting in a U-shaped relation between diffusive CH₄ emissions and Chl-*a* as well as macrophyte cover (Fig. 8). Higher values of annually averaged CH₄ diffusive fluxes occurred at the extreme values of Chl-*a* or of macrophyte cover (minimum or maximum), and lower values occurred at the intermediate values of Chl-*a* or

macrophyte cover. Such U-shape relation resulted from the anti-correlation between macrophyte cover and Chl-*a* (alternative states) and is consistent with reported positive relation between diffusive CH₄ fluxes with both macrophyte cover (e.g. Ray et al., 2023; Theus et al., 2023) as well as with phytoplankton biomass (e.g. DelSontro et al., 2018; Yan et al., 2019; Bartosiewicz et al., 2021). The relative contribution of ebullitive CH₄ fluxes to the total annual CH₄ flux increased with the macrophyte cover (Fig. 86), in agreement with the idea of an increase of CH₄ ebullition relative to diffusive CH₄ emissions in vegetated sediments compared to unvegetated sediments (e.g. Desrosiers et al., 2022; Ray et al., 2023; Theus et al., 2023).

Fluxes of CH₄ and CO₂ have been reported to be negatively related to surface area and depth by numerous studies in ponds (e.g. Holgerson, 2015; Holgerson and Raymond, 2016; Ray et al., 2023; Theus et al., 2023) and lakes (e.g. Kankaala et al., 2013; DelSontro et al., 2018, Deemer and Holgerson, 2021; Casas-Ruiz et al., 2021; Borges et al., 2022). Annual diffusive F_{CH4} and F_{CO2} were both unrelated to surface area and depth in the four studied ponds (Figs. 8, S6) resulting from the narrow range of variation of water depth (0.65 to 1.45 m) and surface area (0.7 to 3.2 ha). The lack of correlation between annual F_{CO2} and both Chl-*a* and macrophyte cover in the four ponds (Fig. S6) might be surprising since other studies have reported lower CO₂ fluxes in more productive lentic systems (e.g. Sand-Jensen and Staehr, 2007; Borges et al., 2022). We hypothesize that given that the four systems were either phytoplankton-dominated or macrophyte-dominated (alternative states), the ponds had an important submerged productivity, in both cases, resulting in a relatively invariant F_{CO2} as function of either Chl-*a* or macrophyte cover. Annual F_{N2O} was negatively correlated with water depth (Fig. S6X) which we hypothesize might reflect a larger dilution of N₂O diffusing from sediments in the deeper systems.

Global average emissions of GHGs in CO₂-eq from inland waters are dominated by CO₂ followed by CH₄ with a small contribution from N₂O according to Lauerwald et al. (2023). However, in small lentic systems such as ponds, the contribution of CH₄ to CO₂-eq emissions can match (e.g. Webb et al., 2023) or dominate (e.g. Ray and Holgerson, 2023; Rabaey and Cotner, 2024) the one of CO₂. The meta-analysis of Holgerson and Raymond (2016) suggested that the CO₂ and CH₄ emissions in CO₂-eq are numerically close in small lentic systems such as ponds but become increasingly dominated by CO₂ emissions with the augmentation of lake size. In the four studied ponds, the GHG emissions in CO₂-eq were dominated by CO₂ and CH₄ with a marginal contribution (<1%) from N₂O (Fig. 9). Annually, CO₂ represented the largest fraction of GHG emissions in CO₂-eq (~60%) in turbid-water ponds (Leybeek and Pêcherries), while CH₄ represented the largest fraction of GHG emissions in CO₂-eq (~60%) in clear-water ponds (Silex and Tenreuken) as a result of higher ebullitive CH₄ fluxes in the clear-water ponds (Fig. 7).

The annual GHG emissions in CO₂-eq increased from 2022 to 2023 due to an increase in the relative contribution of CO₂ diffusive emissions in all four ponds (Fig. 9) as a result of higher precipitations in 2023 (Fig. 2). Air temperatures were similar in both years (annual average of 12.2°C in 2022 and 12.1°C in 2023), and precipitations were 1.5 times higher in 2023 than in 2022. Higher precipitations are likely to increase the inputs of organic and inorganic carbon from soils to ponds by ground-waters, soil-waters, and surface runoff, as previously shown in other lentic systems (e.g. Marotta et al., 2011; Ojala et al., 2011; Rasilo et al., 2012; Vachon and del Giorgio, 2014; Holgerson, 2015). While this hypothesis is only based on the comparison of two years, the increase of the relative contribution of CO₂ diffusive emissions in 2023 was observed in all four ponds which suggests a common uniform driver that would be consistent with a large variation weather such as annual precipitation. The El Niño event in 2023 induced low-level cyclonic wind anomalies and higher precipitation over Western Europe, including Belgium (Chen et al., 2024).

4.5. Conclusions

We found very marked differences in CH₄ dynamics between the two clear-water macrophyte-dominated ponds (Tenreuken and Silex) and the two turbid-water phytoplankton-dominated ponds (Pêcherries and Leybeek) of the city of Brussels. MOX was more important in the two turbid-water ponds compared to the clear-water ponds. MOX correlated to TSM and Chl-*a* concentrations possibly owing to a higher abundance of methanotrophs in the water column fixed to particles and/or an attenuation of light limitation of MOX. Ebullitive CH₄ emissions in 2022-2023 were higher in the two clear-water macrophyte-dominated ponds (Tenreuken and Silex) than in the two turbid-water phytoplankton-dominated ponds (Pêcherries and Leybeek) of the city of Brussels, although, the diffusive CH₄ fluxes were not systematically significantly different between the clear-water ponds and the turbid-water ponds than the two turbid-water ponds, possibly related to high availability of macrophyte organic matter. The annually averaged diffusive N₂O and CO₂ fluxes in 2022-2023 were not significantly statistically different in the two clear-water ponds (Tenreuken and Silex) and in from those in the two turbid-water ponds (Pêcherries and Leybeek). Other studies have found no difference in N₂O sedimentary production in lakes with high and low density of submerged macrophytes. We hypothesize that in human impacted system such as the urban ponds in the city of Brussels, the strong range of variations of DIN was the main driver of N₂O levels and over-rides other possible drivers such as presence or absence of macrophytes. Such a hypothesis was consistent with an overall positive relation between %N₂O and DIN in the urban ponds of the city of Brussels irrespective of presence or absence of macrophytes (Bauduin et al., 2024; this study). We hypothesize that CO₂ fluxes were relatively invariant among the four sampled ponds because of they were of similar size and depth, and that they were all relatively equivalently productive irrespective of whether from phytoplankton or submerged macrophytes.

The total (diffusive and ebullitive) CH₄ emissions represented $57.78 \pm 28.9\%$ (ranging seasonally from 4.9 to 99.9%) of total annual GHG emissions in CO₂-eq in the two clear-water ponds compared to $41.0 \pm 28.7\%$ (ranging seasonally from 2.8 to 99.9%) in the two turbid-water ponds. CO₂ represented nearly all the remainder of total annual GHG emissions in CO₂-eq, and N₂O represented a very marginal fraction ($\leq 0.81 \pm 1.6\%$, ranging from 0.0% to 14.9%, with the maximum coinciding with minimal total CO₂-eq GHG flux in the Leybeek pond).

The seasonal variations of GHG emissions were dominated by CH₄ ebullitive seasonal variations that peaked in summer (both quantitatively and relatively), as CH₄ ebullition was strongly related to water temperature resulting from an increase with water temperature in both flux of bubble and CH₄ content of bubble. The pCO₂ values in the four sampled ponds increased with precipitation at seasonal scale, probably in relation to higher inputs of organic and inorganic carbon by surface runoff. Years 2022 and 2023 were abnormally dry and wet, respectively, and consequently, the GHG emissions were higher in 2023 mainly due to an increase in the relative contribution of CO₂ emissions, probably in response to a strong El Niño event. This would suggest that variations of precipitation also affected year-to-year variations of CO₂ emissions in addition to partly regulating seasonal variations of CO₂ emissions from the four studied ponds.

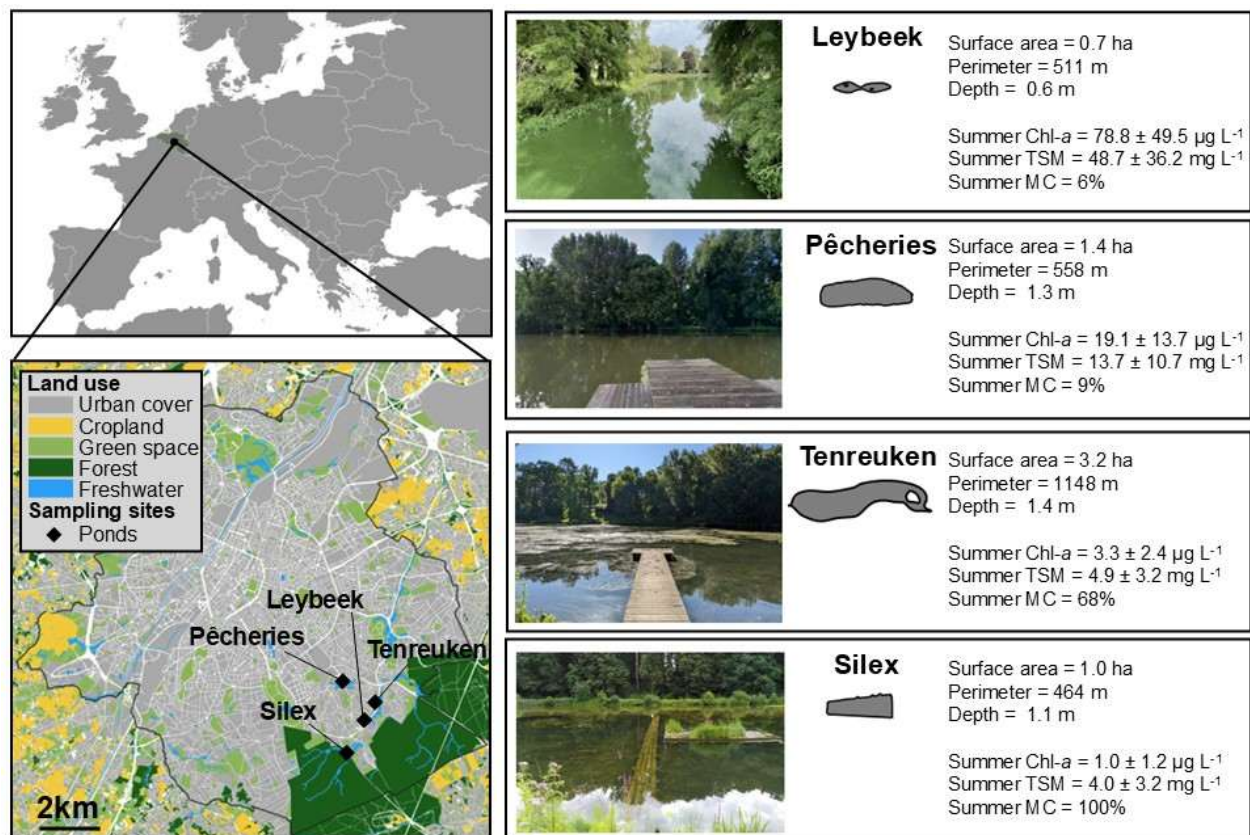


Figure 1: Location of the four sampled urban ponds (black diamonds) in city of Brussels (Belgium, Europe). Bottom-left map shows the metropolitan area of the region of Brussels delineated by the black line and the surrounding region of Flanders in Belgium, showing land cover and sampled urban ponds (black diamonds). The star corresponds to the center of the city (50.8504°N, 4.3487°E). Additional information for each pond is indicated on right panels indicate for each pond the shapes of the ponds, surface area (ha), perimeter (m), average depth (m), mean±standard deviation of summer-chlorophyll-a (Chl-a, in $\mu\text{g L}^{-1}$) and summer total suspended matter (TSM, in mg L^{-1}) in summer (from 21 June to 21 September in 2021, 2022, 2023), and summer total macrophyte cover (MC, in %) (Table S1).

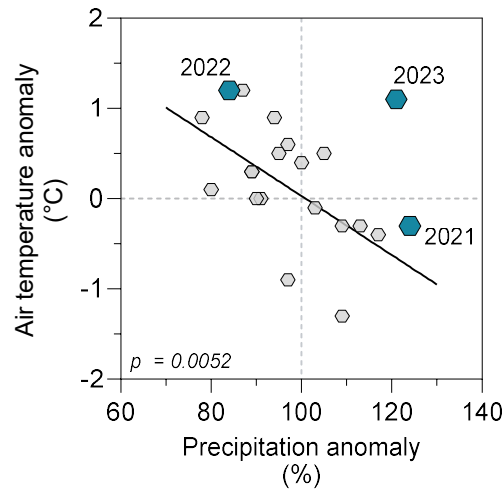
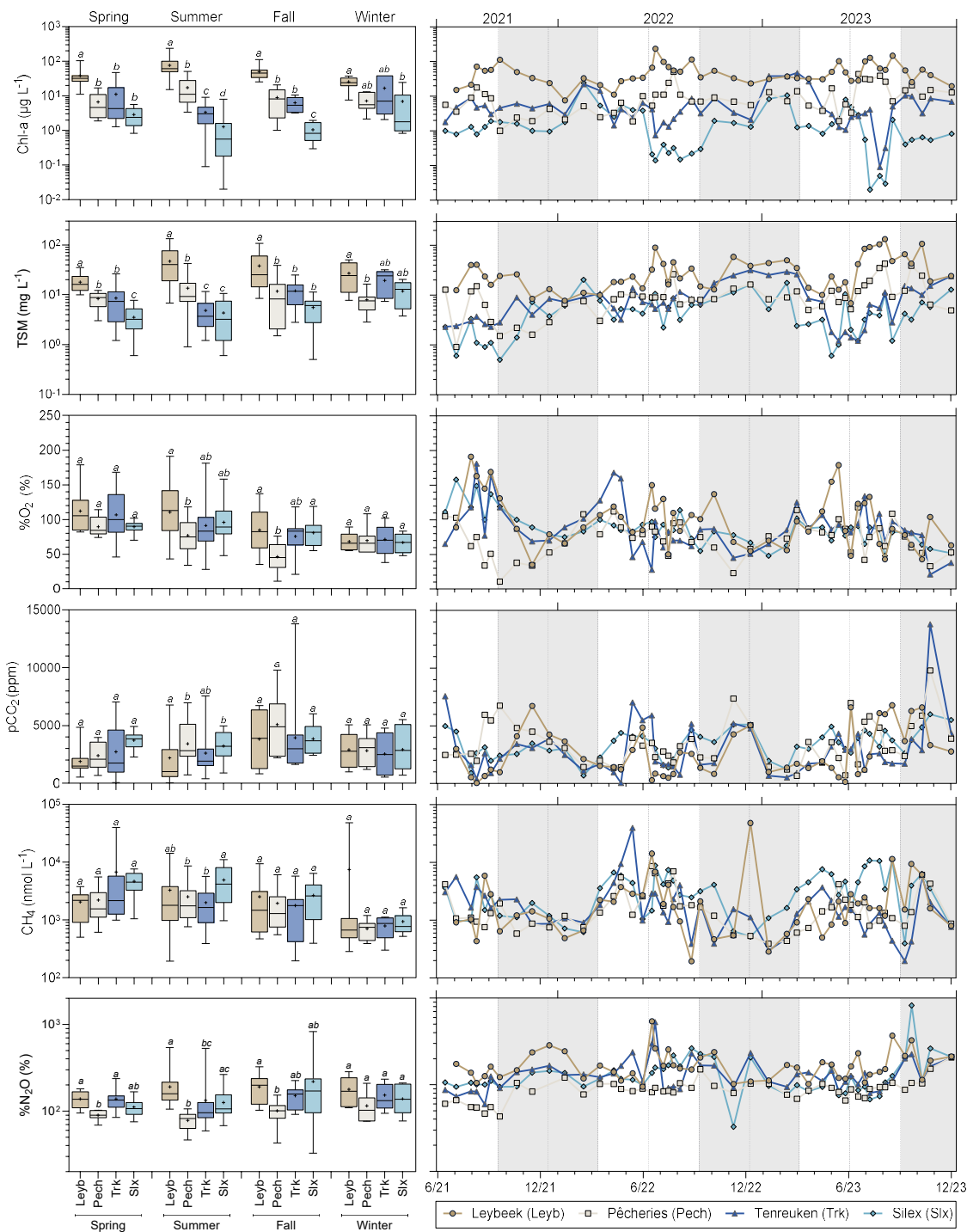


Figure 2: Anomaly of annual Air temperature anomaly (°C) as a function of anomaly of annual precipitation (%) from 2003 to 2023 with respect to average of the 1991-2020 period (difference between the average annual temperature and the normal annual temperature for the reference period 1991-2020 (11 °C), in °C) plotted against precipitation anomaly (ratio between annual precipitation and normal annual precipitation for the reference period 1991-2020 (and 837 mm, respectively), in %) from 2003 to 2023. Each small grey hexagon represents values for years from 2003 to 2020 and larger blue hexagons represent the years of sampling from this study (2021, 2022 and 2023). Linear regression for years 2003-2020 is shown by a black solid line ($Y = 3.29 - 0.03 \cdot X$, $n=20$). Note the anomalous rainy year in 2023 relative to the pattern as function of temperature for the other years, possibly in response to the strong El Niño event of 2023 (Chen et al., 2024).



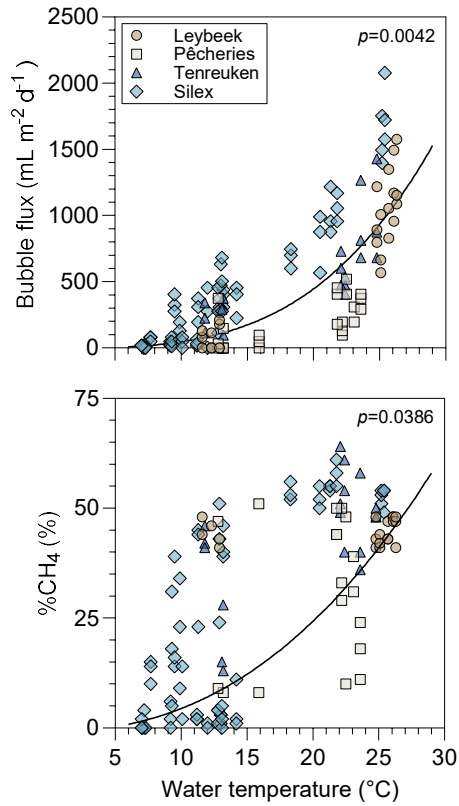
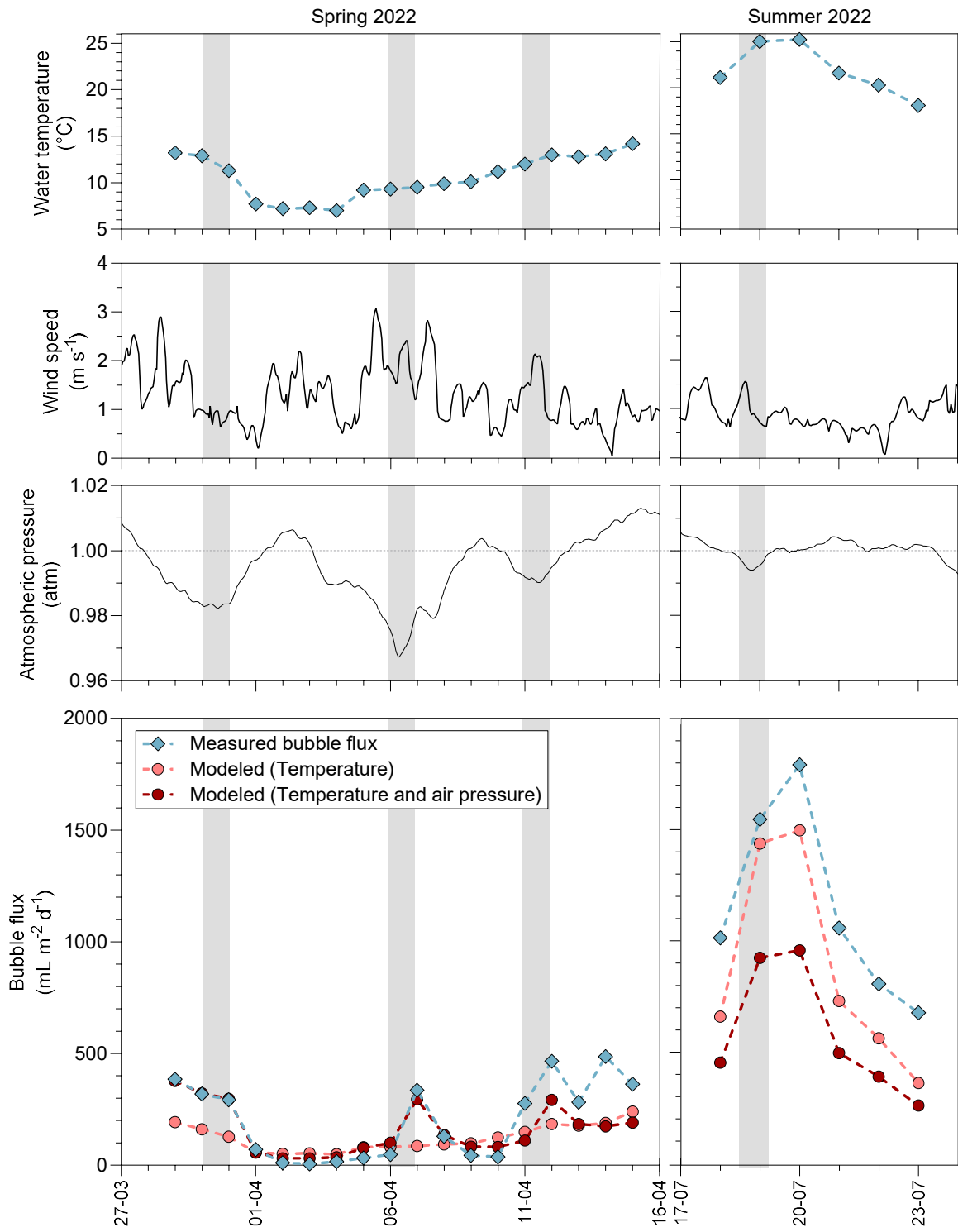


Figure 4: Bubble flux (ml m⁻² d⁻¹) and the relative CH₄ content in bubbles (%CH₄, in %) as a function of surface water temperature (°C) in four urban ponds (Leybeek (Leyb), Pêcherries (Peeh), Tenreuken (Trk), and Silex (Slx)) in the city of Brussels (Belgium) from June 2021 to December 2023. Bubbles fluxes were measured with three bubble traps in spring, summer, and fall of 2022 and 2023, totalling 8 days in the Leybeek, Pêcherries, and Tenreuken ponds and 24 days in the Silex pond. Given the shallowness of the sampled systems (<1.5 m, Fig. 1), we assume that sediments experience the same temperature as surface waters. Solid lines represent the marginal predictions of the GLMM considering the ponds and sampling dates as random effects and the sampling date as an autocorrelation factor for bubble flux as function of water temperature ($Y = 0.0121 \times (1 + X)^{3.4538} - 1$), and %CH₄ as function of water temperature ($Y = 0.0181 \times (1 + X)^{3.3783} - 1$).



941

942 [Figure 5: Surface water temperature \(°C\), wind speed \(m s⁻¹\), atmospheric pressure \(atm\), and measured and modeled bubble](#)
943 [flux \(mL m⁻² d⁻¹\) in the Silex pond from the 29 March 2022 to the 15 April 2022 and from the 18 July 2022 to the 23 July 2022. The](#)
944 [bubble flux was modelled from a fit to data based on water temperature alone and based on from both water temperature and](#)
945 [drops in atmospheric pressure.](#)

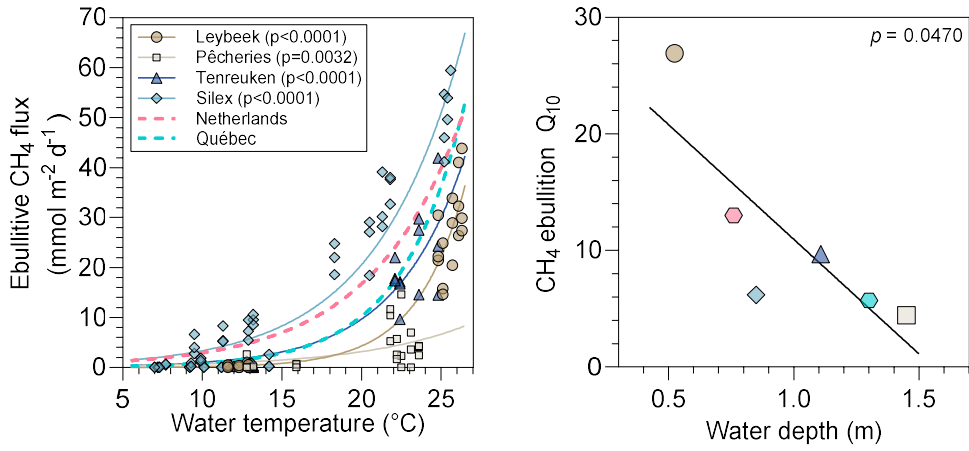


Figure 6: Measured ebullitive CH₄ fluxes (mmol m⁻² d⁻¹) as function of surface water temperature (°C) in four urban ponds (Leybeek, Pêcheres, Tenreuken, and Silex) in the city of Brussels (Belgium), in spring, summer, and fall of 2022 and 2023, totalling 8 days in the Leybeek, Pêcheres, and Tenreuken ponds and 24 days in the Silex pond, with three bubble traps. Solid lines represent exponential fit for the Leybeek ($Y = 0.01 \cdot e^{0.32 \cdot X}$, $n=22$), Pêcheres ($Y = 0.16 \cdot e^{0.15 \cdot X}$, $n=22$), Tenreuken ($Y = 0.10 \cdot e^{0.23 \cdot X}$, $n=19$), Silex ($Y = 0.54 \cdot e^{0.18 \cdot X}$, $n=72$) ponds (Table S7). Dashed lines represent published exponential fit established in similar systems: four small ponds in Québec ($Y = 0.06 \cdot e^{0.25 \cdot X}$) (DeSontro et al., 2016) and a small urban pond in the Netherlands ($Y = 0.51 \cdot e^{0.17 \cdot X}$) (Aben et al., 2017). Each exponential curve allows to determine a Q₁₀ of CH₄ ebullition, plotted against water depth; solid line represents linear regression fit ($Y = 30.64 - 19.67 \cdot X$, $n = 6$).

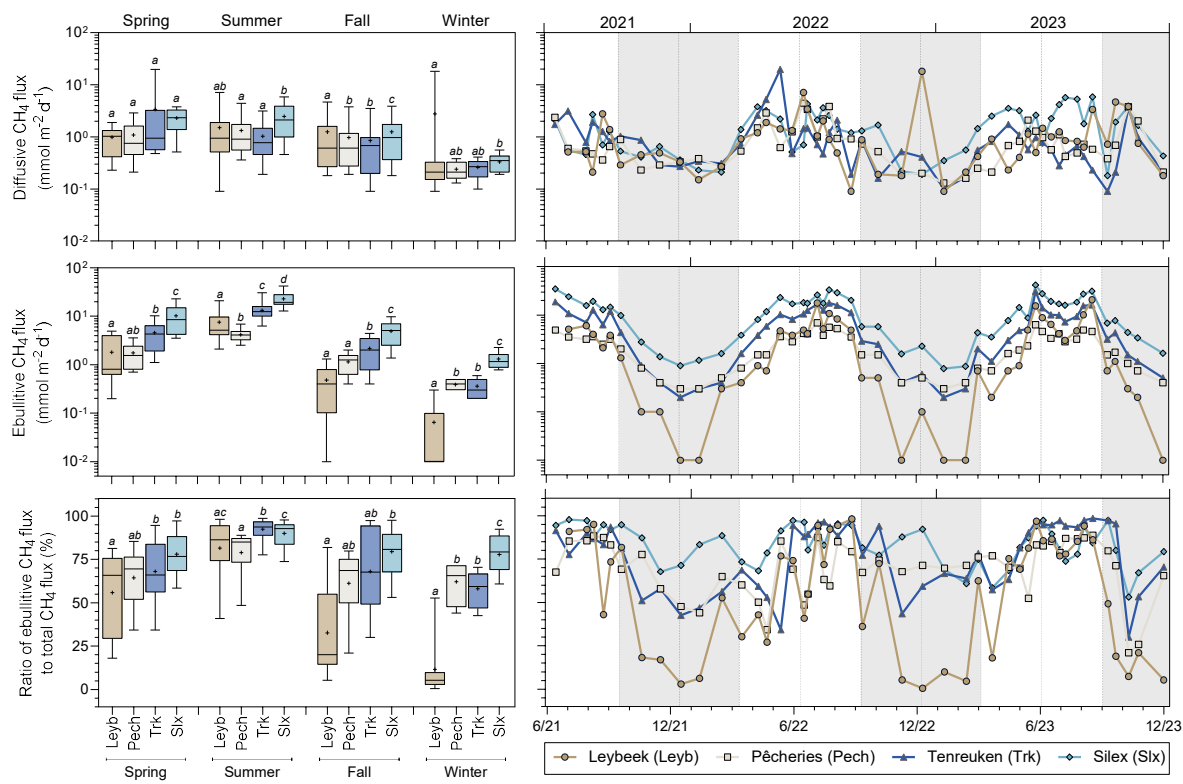


Figure 7: Seasonal variations of diffusive and ebullitive CH_4 fluxes ($\text{mmol m}^{-2} \text{d}^{-1}$), and the ratio of ebullitive CH_4 flux to total (ebullitive+diffusive) CH_4 flux (%) in four urban ponds (Leybeek (Leyb), Pêcheres (Pech), Tenreuken (Trk), and Silex (Slx)) in the city of Brussels (Belgium) from June 2021 to December 2023. Diffusive fluxes were calculated from CH_4 concentration and gas transfer velocity derived from wind speed. Ebullitive CH_4 fluxes were calculated from the relations with water temperature for each pond (Fig. 6; Table S7) from the water temperature data coincident with the diffusive CH_4 fluxes. Box plots show median (horizontal line), mean (cross), and 25–75% percentiles (box limits). Whiskers extend from minimum to maximum values. White and grey bands in the graphs on the right correspond with the autumn/winter and spring/summer periods, respectively, and dotted vertical bars represent the first days of each season. Lower case letters indicate significant differences between ponds (Tables S3 and S4). Data were grouped by season and compared between ponds by repeated measures ANOVA with post-hoc test, results are summarized in Tables S3 and S4. Different lower case letters indicate significant differences between ponds.

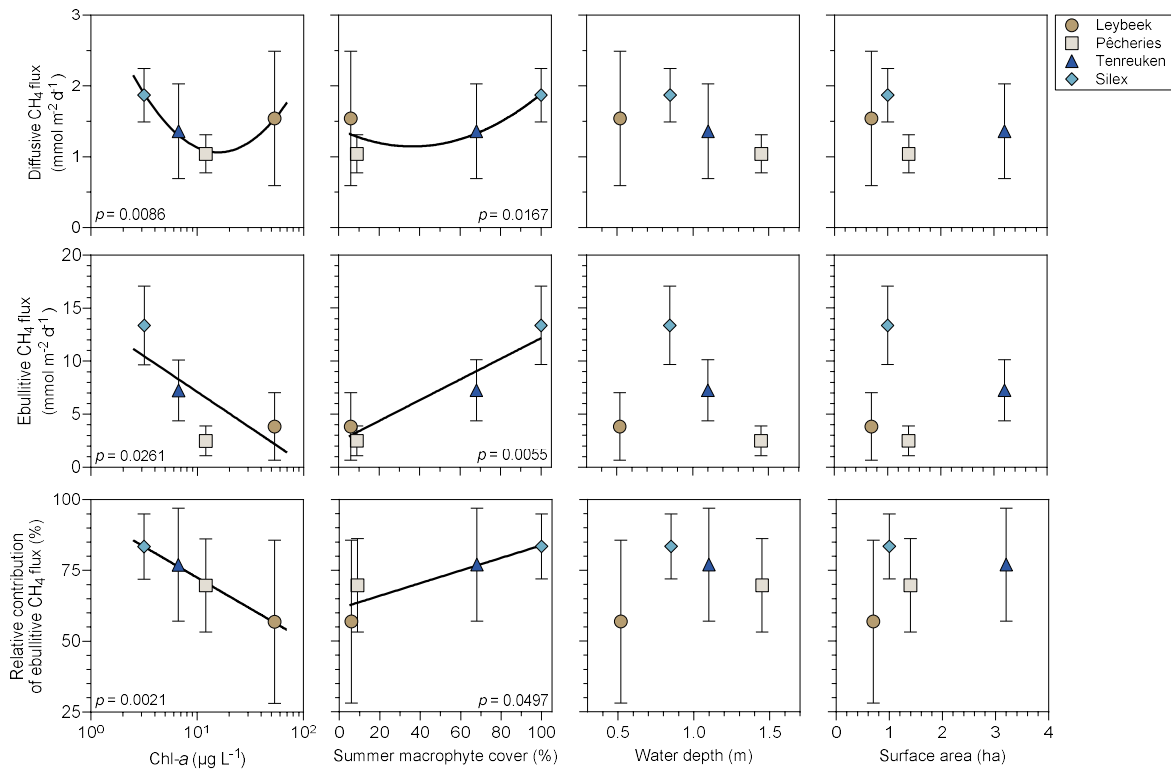


Figure 8: —Mean diffusive and ebullitive CH₄ fluxes (mmol m⁻² d⁻¹) and mean ratio of ebullitive CH₄ flux to total (diffusive+ebullitive) CH₄ flux (%) versus chlorophyll-*a* (Chl-*a*, in µg L⁻¹), total macrophyte cover in summer (%), water depth (m), and lake surface area (ha) in four ponds (Leybeek, Pêcheries, Tenreuken, and Silex) in the city of Brussels (Belgium) from June 2021 to December 2023. Error bars indicate the standard deviation. Dashed/Solid lines indicate trends in relationship between variables/either linear or polynomial fits. Statistical Comparisons between the four ponds for diffusive and ebullitive CH₄ fluxes and mean ratio of ebullitive CH₄ flux to total (diffusive+ebullitive) CH₄ flux are summarized in Table S3.

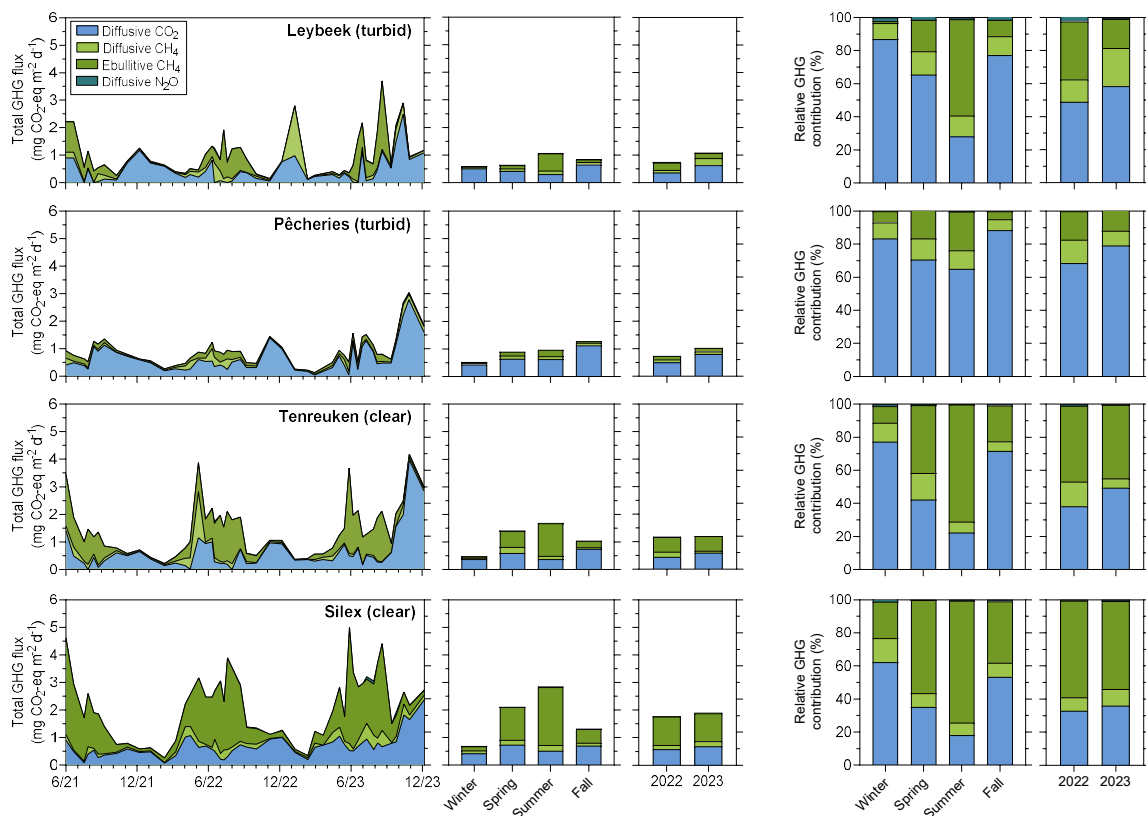


Figure 9: Temporal evolution and relative contribution of emissions to the atmosphere of CO₂ (diffusive), CH₄ (diffusive and ebullitive), and N₂O (diffusive) expressed in CO₂ equivalents (in mg CO₂-eq m⁻² d⁻¹), in four urban ponds (Leybeek, Pêcherries, Tenreuken, and Silex) in the city of Brussels (Belgium) from June 2021 to December 2023. Averages per season include data from 2021, 2022, and 2023. Year 2023 had a higher annual precipitation (1011 mm) than year 2022 (701 mm).

Data availability. ~~Timestamped and georeferenced~~ [the full](https://zenodo.org/record/11103556) data-set is available at 10.5281/zenodo.11103556.

Author contributions. AVB and NG conceived the study; TB collected field samples; TB and AVB made the laboratory analysis; TB and AVB jointly interpreted data and drafted the manuscript with substantial inputs from NG.

Competing interests. The authors declare that they have no conflict of interest.

Acknowledgements. We thank Ozan Efe (University of Liège) and Adriana Anzil (Université Libre de Bruxelles) for analytical assistance, Florence Charlier (Université Libre de Bruxelles) for help in macrophyte identification and density quantification (Table S1), Bruxelles Environnement for providing information on history of operations in the ponds (Table S2), ~~and Cédric Morana (University of Liège) for help and advice in setting up the Picarro G2201-i isotopic analyzer,~~ two anonymous reviewers ~~and Associate Editor (Gabriel Singer)~~ for comments and suggestions on the initial manuscript.

Financial support. TB received funding from the Brussels-Capital Region’s institute for the encouragement of scientific research and innovation (Innoviris) as part of the Smartwater project (RBC/2020-EPF-6 h) and from the “Fonds pour la formation à la Recherche dans l’Industrie et dans l’Agriculture” (FRIA, Belgium). ~~The Picarro G2201-i isotopic analyzer was funded by FRS-FNRS (U.N005.21).~~ AVB is a Research Director at the FRS-FNRS.

References

- Aben, R. C. H., Barros, N., Van Donk, E., Frenken, T., Hilt, S., Kazanjian, G., Lamers, L. P. M., Peeters, E. T. H. M., Roelofs, J.G.M., de Senerpont Domis, L. S., Stephan, S., Velthuis, M., Van de Waal, D., Wik, M., Thornton, B., Wilkinson, J., Delsontro, T., and Kosten, S.: Cross continental increase in methane ebullition under climate change. *Nature communications*, 8(1), 1682. <https://doi.org/10.1038/s41467-017-01535-y>, 2017.
- Audet, J., Neif, É.M., Cao, Y., Hoffmann, C.C., Lauridsen, T.L., Larsen, S.E., Søndergaard, M., Jeppesen, E., and Davidson, T.A.: Heat-wave effects on greenhouse gas emissions from shallow lake mesocosms. *Freshwater Biology*. 2017; 62: 1130–1142. <https://doi.org/10.1111/fwb.12930>, 2017.
- Audet, J., Carstensen, M.V., Hoffmann, C.C., Lavaux, L., Thiemer, K., and Davidson, T.A.: Greenhouse gas emissions from urban ponds in Denmark. *Inland Waters*, 10 (3), 373–385. <https://doi.org/10.1080/20442041.2020.1730680>, 2020.
- Baliña, S., Sanchez, M. L., Izaguirre, I., and del Giorgio, P. A.: Shallow lakes under alternative states differ in the dominant greenhouse gas emission pathways. *Limnology and Oceanography*, 68(1), 1-13. <https://doi.org/10.1002/lno.12243>, 2023.
- Barko, J. W., Gunnison, D., and Carpenter, S. R.: Sediment interactions with submersed macrophyte growth and community dynamics. *Aquatic botany*, 41(1-3), 41-65. [https://doi.org/10.1016/0304-3770\(91\)90038-7](https://doi.org/10.1016/0304-3770(91)90038-7), 1991.
- Bartosiewicz, M., Maranger, R., Przytulska, A., and Laurion, I.: Effects of phytoplankton blooms on fluxes and emissions of greenhouse gases in a eutrophic lake. *Water Research*, 196, 116985. <https://doi.org/10.1016/j.watres.2021.116985>, 2021.
- Bastviken, D., Ejlerstson, J. and Tranvik, L.: Measurement of methane oxidation in lakes: A comparison of methods. *Environmental Science & Technology*, 36, 3354-3361. <https://doi.org/10.1021/es010311p>, 2002.
- Bastviken, D., Treat, C.C., Pangala, S.R., Gauci, V., Enrich-Prast, A., Karlson, M., Gålfalk, M., Romano, M.B., and Sawakuchi, H.O.: The importance of plants for methane emission at the ecosystem scale. *Aquatic Botany*, 184, 103596. <https://doi.org/10.1016/j.aquabot.2022.103596>, 2023.

1016 Bates, D., Maechler, M., Bolker, B., and Walker, S.: Fitting linear mixed-effects models using lme4. *Journal of Statistical*
1017 *Software*, 67, 1–48. <https://doi.org/10.1126/science.1176170>, 2015.

1018 Bauduin, T., Gypens, N., and Borges, A.V.: Seasonal and spatial variations of greenhouse gas (CO₂, CH₄ and N₂O)
1019 emissions from urban ponds in Brussels. *Water Research*, 121257. <https://doi.org/10.1016/j.watres.2024.121257>,
1020 2024.

1021 Borges, A.V., Darchambeau, F., Lambert, T., Morana, C., Allen, G.H., Tambwe, E., and Bouillon, S.: Variations in
1022 dissolved greenhouse gases (CO₂, CH₄, N₂O) in the Congo River network overwhelmingly driven by fluvial-
1023 wetland connectivity. *Biogeosciences*, 16 (19), 3801–3834. <https://doi.org/10.5194/bg-16-3801-2019>, 2019.

1024 Borges, A.V., Deirmendjian, L., Bouillon, S., Okello, W., Lambert, T., Roland, F.A.E., Razanamahandry, V.F., Voarintsoa,
1025 N.R.G., Darchambeau, F., Kimirei, I.A., Descy, J., Allen, G.H., and Morana, C.: Greenhouse gas emissions from
1026 African lakes are no longer a blind spot. *Sciences- Advances*, 8 (25), eabi8716. <https://doi.org/10.1126/sciadv.abi8716>, 2022.

1028 Borges, A.V., Okello, W., Bouillon, S., Deirmendjian, S., Nankabirwa, A., Nabafu, E., Lambert, T., Descy, J-P, and Morana,
1029 C.: Spatial and temporal variations of dissolved CO₂, CH₄ and N₂O in Lakes Edward and George (East Africa).
1030 *Journal of Great Lakes Research*, 49, 229-245, <https://doi.org/10.1016/j.jglr.2022.11.010>, 2023.

1031 Brans, K.I., Engelen, J.M., Souffreau, C., and De Meester, L.: Urban hot-tubs: local urbanization has profound effects on
1032 average and extreme temperatures in ponds. *Landscape and Urban Planning*, 176, 22–29.
1033 <https://doi.org/10.1016/j.landurbplan.2018.04.013>, 2018.

1034 Cael, B. B., Heathcote, A. J., and Seekell, D. A.: The volume and mean depth of Earth's lakes. *Geophysical Research*
1035 *Letters*, 44(1), 209-218. <https://doi.org/10.1002/2016GL071378>, 2017.

1036 Casas-Ruiz, J.P., Jakobsson, J., and del Giorgio, P.A.: The role of lake morphometry in modulating surface water carbon
1037 concentrations in boreal lakes. *Environmental Research Letters*, 16 (7), 074037.
1038 <https://doi.org/10.1088/1748-9326/ac0be3>, 2021.

1039 Chen, B., Zhang, L., and Wang, C.: Distinct impacts of the central and eastern Atlantic Niño on the European climate.
1040 *Geophysical Research Letters*, 51(2), e2023GL107012. <https://doi.org/10.1029/2023GL107012>, 2024.

1041 Choudhury, M. I., McKie, B. G., Hallin, S., and Ecke, F.: Mixtures of macrophyte growth forms promote nitrogen cycling in
1042 wetlands. *Science of the Total Environment*, 635, 1436-1443. <https://doi.org/10.1016/j.scitotenv.2018.04.193>, 2018.

1043 Clifford, C.C., and Heffernan, J.B.: Artificial aquatic ecosystems. *Water*, 10 (8), 1096. <https://doi.org/10.3390/w10081096>,
1044 2018.

1045 Codispoti, L.A., and Christensen, J.P.: Nitrification, denitrification and nitrous oxide cycling in the eastern tropical South
1046 Pacific Ocean. *Marine Chemistry*, 16 (4), 277–300. [https://doi.org/10.1016/0304-4203\(85\)90051-9](https://doi.org/10.1016/0304-4203(85)90051-9),
1047 1985.

1048 Cole, J.J., and Caraco, N.F.: Atmospheric exchange of carbon dioxide in a low-wind oligotrophic lake measured by the
1049 addition of SF₆. *Limnology and Oceanography*, 43 (4), 647–656.
1050 <https://doi.org/10.4319/lo.1998.43.4.0647>, 1998.

1051 Dan, Z., Chuan, W., Qiaohong, Z., and Xingzhong, Y.: Sediments nitrogen cycling influenced by submerged macrophytes
1052 growing in winter. *Water Science and Technology*, 83(7), 1728-1738. <https://doi.org/10.2166/wst.2021.081>, 2021.

1053 Davidson, T.A., Audet, J., Svenning, J.C., Lauridsen, T.L., Søndergaard, M., Landkildehus, F., and Jeppesen, E.:
1054 Eutrophication effects on greenhouse gas fluxes from shallow-lake mesocosms override those of climate warming.
1055 *Global Change Biology*, 21 (12), 4449–4463. <https://doi.org/10.1111/gcb.13062>, 2015.

1056 Deemer, B. R., and Holgerson, M. A.: Drivers of methane flux differ between lakes and reservoirs, complicating global
1057 upscaling efforts. *Journal of Geophysical Research: Biogeosciences*, 126(4) <https://doi.org/10.1029/2019JG005600>
1058 , 2021.

1059 DelSontro, T., Beaulieu, J. J., and Downing, J. A.: Greenhouse gas emissions from lakes and impoundments: Upscaling in
1060 the face of global change. *Limnology and Oceanography Letters*, 3(3), 64-75. <https://doi.org/10.1002/lol2.10073>,
1061 2018.

1062 DelSontro, T., Kunz, M. J., Kempter, T., Wüest, A., Wehrli, B., and Senn, D. B.: Spatial Heterogeneity of Methane
1063 Ebullition in a Large Tropical Reservoir, *Environmental Science & Technology*, 45 (23), 9866-9873,
1064 <https://doi.org/10.1021/es2005545>, 2011.

1065 DelSontro, T., Boutet, L., St-Pierre, A., del Giorgio, P.A., and Prairie, Y.T.: Methane ebullition and diffusion from northern
1066 ponds and lakes regulated by the interaction between temperature and system productivity, *Limnology and*
1067 *Oceanography*, *Limnol. Oceanogr.* 61(S1), S62-S77 <https://doi.org/10.1002/lno.10335>, 2016.

1068 Deng, Hg., Zhang, J., Wu, J., Yao, X., and Yang, L.-W.: Biological denitrification in a macrophytic lake: implications for
1069 macrophytes-dominated lake management in the north of China. *Environmental Sciences and Pollution Research*,
1070 27, 42460–42471. <https://doi.org/10.1007/s11356-020-10230-3>, 2020.

1071 Desrosiers, K., DelSontro, T., and del Giorgio, P.A.: Disproportionate Contribution of Vegetated Habitats to the CH₄ and
1072 CO₂ Budgets of a Boreal Lake. *Ecosystems*, 1-20. <https://doi.org/10.1007/s10021-021-00730-9>, 2022.

1073 Dickson, A.G.; Sabine, C.L. and Christian, J.R.: Guide to best practices for ocean CO₂ measurement. Sidney, British
1074 Columbia, North Pacific Marine Science Organization, 191pp. (PICES Special Publication 3; IOCCP Report 8).
1075 <https://doi.org/10.25607/OBP-1342>, 2007.

1076 Dutton, G., Elkins II, J., Hall, B., NOAA ESRL, Earth System Research Laboratory Halocarbons and Other Atmospheric
1077 Trace Gases Chromatograph for Atmospheric Trace Species (CATS) Measurements. NOAA National Centers for
1078 Environmental Information. <https://doi.org/10.7289/V5X0659V>. Version 1. [Database: atmospheric nitrous oxide
1079 N₂O] [2024-03–27], 2023.

1080 Goeckner, A. H., Lusk, M. G., Reisinger, A. J., Hosen, J. D., and Smoak, J. M.: Florida's urban stormwater ponds are net
1081 sources of carbon to the atmosphere despite increased carbon burial over time. *Communications earth &*
1082 *environment*, 3(1), 53, <https://doi.org/10.1038/s43247-022-00384-y> 2022.

1083 Gorsky, A. L., Dugan, H. A., Wilkinson, G. M., and Stanley, E. H.: Under-ice oxygen depletion and greenhouse gas
1084 supersaturation in north temperate urban ponds. *Journal of Geophysical Research: Biogeosciences*, 129(6),
1085 <https://doi.org/10.1029/2024JG008120>, 2024.

1086 Gorsky, A.L., Racanelli, G.A., Belvin, A.C., and Chambers, R.M.: Greenhouse gas flux from stormwater ponds in
1087 southeastern Virginia (USA). *Anthropocene*, 28, 100218. <https://doi.org/10.1016/j.ancene.2019.100218>, 2019.

1088 Grasset, C., Abril, G., Mendonça, R., Roland, F., and Sobek, S.: The transformation of macrophyte-derived organic matter to
1089 methane relates to plant water and nutrient contents. *Limnology and Oceanography*, 64(4), 1737-1749,
1090 <https://doi.org/10.1002/lno.11148>, 2019.

1091 Grasset, C., Sobek, S., Scharnweber, K., Moras, S., Villwock, H., Andersson, S., Hiller, C., Nydahl, A.C., Chaguaceda, F.,
1092 Colom, W., and Tranvik, L.J.: The CO₂-equivalent balance of freshwater ecosystems is non-linearly related to
1093 productivity. *Global Change Biology*, *Glob. Chang. Biol.* 26 (10), 5705–5715. <https://doi.org/10.1111/gcb.15284>,
1094 2020.

1095 Grasshoff, K., and Johannsen, H.: A new sensitive and direct method for the automatic determination of ammonia in sea
1096 water. *ICES Journal of Marine Science*, *ICES J. Mar. Sci.* 34 (3), 516–521. <https://doi.org/10.1093/icesjms/34.3.516>,
1097 1972.

1098 Grasshoff, K., Kremling, K., and Ehrhardt, M.: Methods of Seawater Analysis: Determination of Nitrite. John Wiley & Sons,
1099 2009.

1100 Grinham, A., Albert, S., Deering, N., Dunbabin, M., Bastviken, D., Sherman, B., Lovelock, C.E., and Evans, C.D.: The
1101 importance of small artificial water bodies as sources of methane emissions in Queensland, Australia. *Hydrology*
1102 *and Earth System Sciences*, *Hydrol. Earth Syst. Sci.* 22 (10), 5281–5298. <https://doi.org/10.5194/hess-22-5281-2018>,
1103 2018.

- 1104 Harpenslager, S. F., Thieme, K., Levertz, C., Misteli, B., Sebola, K. M., Schneider, S. C., Hilt, S., and Köhler, J.: Short-term
1105 effects of macrophyte removal on emission of CO₂ and CH₄ in shallow lakes. *Aquatic Botany*, 182, 103555.
1106 <https://doi.org/10.1016/j.aquabot.2022.103555>, 2022.
- 1107 Hassall, C., The ecology and biodiversity of urban ponds. *WIREs Water*, 1: 187-206. <https://doi.org/10.1002/wat2.1014>,
1108 2014.
- 1109 Herrero Ortega, S., Romero González-Quijano, C., Casper, P., Singer, G.A., and Gessner, M.O.: Methane emissions from
1110 contrasting urban freshwaters: rates, drivers, and a whole-city footprint. *Global change biology*, 25 (12), 4234–4243. <https://doi.org/10.1111/gcb.14799>, 2019.
1111
- 1112 Hilt, S., Brothers, S., Jeppesen, E., Veraart, A. J., and Kosten, S.: Translating regime shifts in shallow lakes into changes in
1113 ecosystem functions and services. *BioScience*, 67(10), 928-936. <https://doi.org/10.1093/biosci/bix106>, 2017.
- 1114 Holgerson, M., and Raymond, P.: Large contribution to inland water CO₂ and CH₄ emissions from very small ponds. *Nature*
1115 *Geoscience*, 9, 222–226. <https://doi.org/10.1038/ngeo2654>, 2016.
- 1116 Holgerson, M.A.: Drivers of carbon dioxide and methane supersaturation in small, temporary ponds, *Biogeochemistry*, 124,
1117 305–318. <https://doi.org/10.1007/s10533-015-0099-y>, 2015.
- 1118 Huttunen, J. T., Alm, J., Liikanen, A., Juutinen, S., Larmola, T., Hammar, T., Silvola, T., and Martikainen, P. J.: Fluxes of
1119 methane, carbon dioxide and nitrous oxide in boreal lakes and potential anthropogenic effects on the aquatic
1120 greenhouse gas emissions. *Chemosphere*, 52(3), 609-621. [https://doi.org/10.1016/S0045-6535\(03\)00243-1](https://doi.org/10.1016/S0045-6535(03)00243-1), 2003.
- 1121 Hyvönen, T., Ojala, A., Kankaala, P., & Martikainen, P. J.: Methane release from stands of water horsetail (*Equisetum*
1122 *fluviatile*) in a boreal lake, *Freshwater Biology*, 40, 275– 284. <https://doi.org/10.1046/j.1365-2427.1998.00351.x>,
1123 1998.
- 1124 Johnson, M.S., Matthews, E., Du, J., Genovese, V., and Bastviken, D.: Methane Emission from Global Lakes: New
1125 Spatiotemporal Data and Observation-Driven Modeling of Methane Dynamics Indicates Lower Emissions. *Journal*
1126 *of Geophysical Research: Biogeosciences*, 127(7). <https://doi.org/10.1029/2022JG006793>, 2022.
- 1127 Juutinen, S., Alm, J., Larmola, T., Huttunen, J. T., Morero, M., Martikainen, P. J., and Silvola, J.: Major implication of the
1128 littoral zone for methane release from boreal lakes, *Global biogeochemical cycles*, 17(4), 1117, <https://doi.org/10.1029/2003GB002105>, 2003.
1129
- 1130 Kankaala, P., Huotari, J., Tulonen, T., and Ojala, A.: A Lake-size dependent physical forcing drives carbon dioxide and
1131 methane effluxes from lakes in a boreal landscape. *Limnology and Oceanography*, 58:1915–1930.
1132 <https://doi.org/10.4319/lo.2013.58.6.1915>, 2013.
- 1133 Keller, M., and Stallard, R. F.: Methane emission by bubbling from Gatun Lake, Panama, *Journal of Geophysical Research:*
1134 *Atmospheres*, 99(D4), 8307–8319, doi:10.1029/92JD02170, 1994.
- 1135 Koroleff, J.: Determination of total phosphorus by alkaline persulphate oxidation. *Methods of Seawater Analysis*. Verlag
1136 Chemie, Weinheim, pp. 136–138, 1983.
- 1137 Kosten, S., Roland, F., Da Motta Marques, D. M., Van Nes, E. H., Mazzeo, N., Sternberg, L. D. S., Scheffer, M., and Cole,
1138 J. J. Climate-dependent CO₂ emissions from lakes. *Global Biogeochemical Cycles*, 24(2).
1139 <https://doi.org/10.1029/2009GB003618>, 2010.
- 1140 Lan, X., K.W. Thoning, and E.J. Dlugokencky: Trends in globally-averaged CH₄, N₂O, and SF₆ determined from NOAA
1141 Global Monitoring Laboratory measurements [data set]. Version 2024-08, <https://doi.org/10.15138/P8XG-AA10>,
1142 2024.
- 1143 Lauerwald, R., Regnier, P., Figueiredo, V., Enrich-Prast, A., Bastviken, D., Lehner, B., Maavara, T., and Raymond, P.:
1144 Natural Lakes Are a Minor Global Source of N₂O to the Atmosphere. *Global Biogeochemical Cycles*, 33(12),
1145 1564–1581. <https://doi.org/10.1029/2019GB006261>, 2019.
- 1146 Lauerwald, R., Allen, G. H., Deemer, B. R., Liu, S., Maavara, T., Raymond, P., Alcott, L., Bastviken, D., Hastie, A.,
1147 Holgerson, M.A., Johnson, M. S., Lehner, B., Lin, P., Marzadri, A., Ran, L., Tian, H., Yang, X., Yao, Y., and

1148 Regnier, P.: Inland water greenhouse gas budgets for RECCAP2: 2. Regionalization and homogenization of
1149 estimates. *Global Biogeochemical Cycles*, 37, e2022GB007658. <https://doi.org/10.1029/2022GB007658>, 2023.

1150 Liu, W., Jiang, X., Zhang, Q., Li, F., and Liu, G.: Has submerged vegetation loss altered sediment denitrification, N₂O
1151 production, and denitrifying microbial communities in subtropical lakes? *Global Biogeochemical Cycles*, 32, 1195–
1152 1207. <https://doi.org/10.1029/2018GB005978>, 2018.

1153 Maavara, T., Lauerwald, R., Laruelle, G. G., Akbarzadeh, Z., Bouskill, N. J., Van Cappellen, P., and Regnier, P.: Nitrous
1154 oxide emissions from inland waters: Are IPCC estimates too high? *Global Change Biology*, 25(2), 473–488.
1155 <https://doi.org/10.1111/gcb.145042>, 2019.

1156 Marotta, H., Duarte, C. M., Pinho, L., and Enrich-Prast, A.: Rainfall leads to increased pCO₂ in Brazilian coastal lakes.
1157 *Biogeosciences*, 7(5), 1607–1614. <https://doi.org/10.5194/bg-7-1607-2010>, 2010.

1158 Martinez-Cruz, K., Gonzalez-Valencia, R., Sepulveda-Jauregui, A., Plascencia- Hernandez, F., Belmonte-Izquierdo, Y., and
1159 Thalasso, F.: Methane emission from aquatic ecosystems of Mexico City. *Aquatic Sciences, Aquat. Sci.* 79, 159–
1160 169. <https://doi.org/10.1007/s00027-016-0487-y>, 2017.

1161 Mengis, M., Gächter, R., and Wehrli, B.: Sources and sinks of nitrous oxide (N₂O) in deep lakes. *Biogeochemistry*, 38, 281–
1162 301. <https://doi.org/10.1023/A:1005814020322>, 1997.

1163 Myrhe, G., Shindell, D., Bréon, F.M., Collins, W., and Al, E. Anthropogenic and natural radiative forcing. Climate Change
1164 2013 the Physical Science Basis: working Group I Contribution to the Fifth Assessment Report of the
1165 Intergovernmental Panel on Climate Change. Chapter 8 : Anthropogenic and Natural Radiative Forcing
1166 9781107057, 659–740. <https://doi.org/10.1017/CBO9781107415324.018>, 2013.

1167 Natchimuthu, S., Panneer Selvam, B., and Bastviken, D.: Influence of weather variables on methane and carbon dioxide flux
1168 from a shallow pond. *Biogeochemistry*, 119, 403–413. <https://doi.org/10.1007/s10533-014-9976-z>, 2014.

1169 Natchimuthu, S., Sundgren, I., Gålfalk, M., Klemetsson, L., Crill, P., Danielsson, Å. and Bastviken, D. (2016), Spatio-
1170 temporal variability of lake CH₄ fluxes and its influence on annual whole lake emission estimates. *Limnology and*
1171 *Oceanography*, 61: S13-S26. <https://doi.org/10.1002/lno.10222>, 2016.

1172 Ni, M., Liang, X., Hou, L., Li, W., and He, C.: Submerged macrophytes regulate diurnal nitrous oxide emissions from a
1173 shallow eutrophic lake: A case study of Lake Wuliangsu in the temperate arid region of China. *Science of The*
1174 *Total Environment*, 811, 152451. <https://doi.org/10.1016/j.scitotenv.2021.152451>, 2022.

1175 Ojala A., Bellido J.L., Tulonen T., Kankaala P., and Huotari J.: Carbon gas fluxes from a brown-water and a clear-water lake
1176 in the boreal zone during a summer with extreme rain events, *Limnology and Oceanography*, 56,
1177 <https://doi.org/10.4319/lo.2011.56.1.0061>, 2011.

1178 Ollivier, Q.R., Maher, D.T., Pitfield, C., and Macreadie, P.I.: Punching above their weight: large release of greenhouse gases
1179 from small agricultural dams. *Global change biologyGlob. Chang. Biol.* 25 (2), 721–732.
1180 <https://doi.org/10.1111/gcb.14477>, 2019.

1181 Peacock, M., Audet, J., Bastviken, D., Cook, S., Evans, C.D., Grinham, A., Holgerson, M. A., Högbom, L., Pickard, A.E.,
1182 Zieliński, P., and Futter, M.N.: Small artificial waterbodies are widespread and persistent emitters of methane and
1183 carbon dioxide. *Global change biologyGlob. Chang. Biol.* 27 (20), 5109–5123. <https://doi.org/10.1111/gcb.15762>,
1184 2021.

1185 Peacock, M., Audet, J., Jordan, S., Smeds, J., and Wallin, M.B.: Greenhouse gas emissions from urban ponds are driven by
1186 nutrient status and hydrology. *Ecosphere*, 10 (3), e02643. <https://doi.org/10.1002/ecs2.2643>, 2019.

1187 Peretyatko, A., Symoens, J. J., and Triest, L.: Impact of macrophytes on phytoplankton in eutrophic peri-urban ponds,
1188 implications for pond management and restoration. *Belgian Journal of Botany*, 83-99.
1189 <https://doi.org/10.2307/20794626>, 2007.

1190 R Core Team (2021). R: A language and environment for statistical computing. R Foundation for Statistical Computing,
1191 Vienna, Austria. <https://www.R-project.org/>, 2021.

- 1192 Rabaey, J. and Cotner, J.: Pond greenhouse gas emissions controlled by duckweed coverage. *Frontiers in environmental*
1193 *science, Front. Environ. Sci.* 10, 889289 <https://doi.org/10.3389/fenvs2022.889289>, 2022.
- 1194 Rabaey, J. and Cotner, J.: The influence of mixing on seasonal carbon dioxide and methane fluxes in ponds.
1195 *Biogeochemistry*, 1-18, <https://doi.org/10.1007/s10533-024-01167-7>, 2024.
- 1196 Rasilo, T., Ojala, A., Huotari, J. and Pumpanen, J.: Rain Induced Changes in Carbon Dioxide Concentrations in the Soil–
1197 Lake–Brook Continuum of a Boreal Forested Catchment. *Vadose Zone Journal*, 11: vzj2011.0039.
1198 <https://doi.org/10.2136/vzj2011.0039>, 2012.
- 1199 Ray, N. E., and Holgerson, M. A.: High Intra-Seasonal Variability in Greenhouse Gas Emissions from Temperate
1200 Constructed Ponds. *Geophysical Research Letters*, 50(18), e2023GL104235,
1201 <https://doi.org/10.1029/2023GL104235>, 2023.
- 1202 Ray, N. E., Holgerson, M. A., Andersen, M. R., Bikše, J., Bortolotti, L. E., Futter, M., Kokorite, I., Law, A., McDonald, C.,
1203 Mesman, J.P., Peacock, M., Richardson, D.C., Arsenault, J., Bansal, S., Cawley, K., Kuhn, M., Shahabinia, A.R.,
1204 and Smufer, F.: Spatial and temporal variability in summertime dissolved carbon dioxide and methane in
1205 temperate ponds and shallow lakes. *Limnology and Oceanography*, 68(7), 1530-1545.
1206 <https://doi.org/10.1002/lno.12362>, 2023.
- 1207 Raymond, P. A., Hartmann, J., Lauerwald, R., Sobek, S., McDonald, C., Hoover, M., Butman, D., Striegl, R., Mayorga, E.,
1208 Humborg, C., Kortelainen, P., Dürr, H., Meybeck, M., Ciais, P., and Guth, P.: Global carbon dioxide emissions
1209 from inland waters. *Nature*, 503(7476), 355–359. <https://doi.org/10.1038/nature12760>, 2013.
- 1210 Reitsema, R. E., Meire, P., and Schoelynck, J.: The future of freshwater macrophytes in a changing world: dissolved organic
1211 carbon quantity and quality and its interactions with macrophytes. *Frontiers in Plant Science*, 9, 301954.
1212 <https://doi.org/10.3389/fpls.2018.00629>, 2018.
- 1213 Rocher-Ros, G., Stanley, E. H., Loken, L. C., Casson, N. J., Raymond, P. A., Liu, S., Amatulli, G., and Sponseller, R. A.:
1214 Global methane emissions from rivers and streams. *Nature*, 621:530–535. [https://doi.org/10.1038/s41586-023-](https://doi.org/10.1038/s41586-023-06344-6)
1215 [06344-6](https://doi.org/10.1038/s41586-023-06344-6), 2023.
- 1216 Rosentreter, J. A., Borges, A. V., Deemer, B. R., Holgerson, M. A., Liu, S., Song, C., Melack, J., Raymond, P. A., Duarte, C.
1217 M., Allen, G. H., Olefeldt, D., Poulter, B., Battin, T. L., and Eyre, B. D.: Half of global methane emissions come
1218 from highly variable aquatic ecosystem sources. *Nature Geoscience*, 14(4), 225–230.
1219 <https://doi.org/10.1038/s41561-021-00715-2>, 2021.
- 1220 Sand-Jensen, K., & Staehr, P. A.: Scaling of pelagic metabolism to size, trophic and forest cover in small Danish lakes.
1221 *Ecosystems*, 10, 128-142. <https://doi.org/10.1007/s10021-006-9001-z>, 2007.
- 1222 Scandella, B. P., Varadharajan, C., Hemond, H. F., Ruppel, C., and Juanes, R.: A conduit dilation model of methane venting
1223 from lake sediments. *Geophysical Research Letters*, 38(6). <https://doi.org/10.1029/2011GL046768>, 2011.
- 1224 Scheffer, M., Hosper, S. H., Meijer, M. L., Moss, B., and Jeppesen, E.: Alternative equilibria in shallow lakes. *Trends in*
1225 *ecology & evolution*, 8(8), 275-279. [https://doi.org/10.1016/0169-5347\(93\)90254-M](https://doi.org/10.1016/0169-5347(93)90254-M), 1993.
- 1226 Schulz, S. and Conrad, R.: Influence of temperature on pathways to methane production in the permanently cold profundal
1227 sediment of Lake Constance. *FEMS Microbiology Ecology*, 20 1-14; [https://doi.org/10.1111/j.1574-](https://doi.org/10.1111/j.1574-6941.1996.tb00299.x)
1228 [6941.1996.tb00299.x](https://doi.org/10.1111/j.1574-6941.1996.tb00299.x), 1996.
- 1229 Singh, S.N., Kulshreshtha, K., and Agnihotri, S.: Seasonal dynamics of methane emission from wetlands. *Chemosphere-*
1230 *Global Change Science, Chemosphere—Glob. Chang.—Sci.* 2 (1), 39–46. [https://doi.org/10.1016/S1465-](https://doi.org/10.1016/S1465-9972(99)00046-X)
1231 [9972\(99\)00046-X](https://doi.org/10.1016/S1465-9972(99)00046-X), 2000.
- 1232 Stanley, E. H., Casson, N. J., Christel, S. T., Crawford, J. T., Loken, L. C., and Oliver, S. K.: The ecology of methane in
1233 streams and rivers: patterns, controls, and global significance. *Ecological Monographs*, 86(2), 146–171.
1234 <https://doi.org/10.1890/15-1027>, 2016.
- 1235 Taoka, T., Iwata, H., Hirata, R., Takahashi, Y., Miyabara, Y., and Itoh, M.: Environmental controls of diffusive and
1236 ebullitive methane emissions at a subdaily time scale in the littoral zone of a midlatitude shallow lake. *Journal of*
1237 *Geophysical Research: Biogeosciences*, 125, e2020JG005753. <https://doi.org/10.1029/2020JG005753>, 2020.

1238 Theus, M. E., Ray, N. E., Bansal, S., and Holgerson, M. A.: Submersed macrophyte density regulates aquatic greenhouse gas
1239 emissions. *Journal of Geophysical Research: Biogeosciences*, 128(10), <https://doi.org/10.1029/2023JG007758>,
1240 2023.

1241 Tixier, G., M Lafont, M., L Grapentine, L., Q Rochfort, Q., and J Marsalek, J.: Ecological risk assessment of urban
1242 stormwater ponds: Literature review and proposal of a new conceptual approach providing ecological quality goals
1243 and the associated bioassessment tools, *Ecological Indicators*, 11, 1497-1506,
1244 <https://doi.org/10.1016/j.ecolind.2011.03.027>, 2011.

1245 Tokida, T., Miyazaki, T., Mizoguchi, M., Nagata, O., Takakai, F., Kagemoto, A., and Hatano, R.: Falling atmospheric
1246 pressure as a trigger for methane ebullition from peatland. *Global Biogeochemical Cycles*, 21(2).
1247 <https://doi.org/10.1029/2006GB002790>, 2007.

1248 Vachon, D., and del Giorgio, P.A. Whole-Lake CO₂ Dynamics in Response to Storm Events in Two Morphologically
1249 Different Lakes. *Ecosystems*, 17, 1338–1353 (2014). <https://doi.org/10.1007/s10021-014-9799-8>, 2014.

1250 Vachon, D., Langenegger, T., Donis, D., Beaubien, S. E., and McGinnis, D. F.: Methane emission offsets carbon dioxide
1251 uptake in a small productive lake. *Limnology and Oceanography Letters*, 5(6), 384-392,
1252 <https://doi.org/10.1002/lol2.10161>, 2020.

1253 van Bergen, T.J.H.M., Barros, N., Mendonça, R., Aben, R.C.H., Althuisen, I.H.J., Huszar, V., Lamers, L.P.M., Lüring, M.,
1254 Roland, F., and Kosten, S.: Seasonal and diel variation in greenhouse gas emissions from an urban pond and its
1255 major drivers. *Limnology and Oceanography: Limnol.—Oceanogr.* 64 (5), 2129–2139.
1256 <https://doi.org/10.1002/lno.11173>, 2019.

1257 Varadharajan, C., and Hemond, H. F.: Time - series analysis of high - resolution ebullition fluxes from a stratified,
1258 freshwater lake. *Journal of Geophysical Research: Biogeosciences*, 117(G2).
1259 <https://doi.org/10.1029/2011JG001866>, 2012.

1260 Velthuis, M., and Veraart, A. J.: Temperature sensitivity of freshwater denitrification and N₂O emission—A meta-analysis.
1261 *Global Biogeochemical Cycles*, 36(6), <https://doi.org/10.1029/2022GB007339>, 2022.

1262 Verpoorter, C., Kutser, T., Seekell, D. A., and Tranvik, L. J.: A global inventory of lakes based on high - resolution satellite
1263 imagery. *Geophysical Research Letters*, 41(18), 6396-6402. <https://doi.org/10.1002/2014GL060641>, 2014.

1264 Wang, G., Xia, X., Liu, S., Zhang, S., Yan, W., McDowell, W.H.: Distinctive Patterns and Controls of Nitrous Oxide
1265 Concentrations and Fluxes from Urban Inland Waters, *Environmental Science & Technology* Environ.-Sci.-Technol.,
1266 55, 8422–8431, <https://doi.org/10.1021/acs.est.1c00647>, 2021.

1267 Wanninkhof, R.: Relationship between gas exchange and wind speed over the ocean. *Journal of Geophysical Research:*
1268 *Oceans, J. Geophys. Res.* 97, 7373–7381. <https://doi.org/10.1029/92JC00188>, 1992.

1269 Webb, J.R., Clough, T.J., Quayle, W.C.: A review of indirect N₂O emission factors from artificial agricultural waters,
1270 *Environmental Research Letters* Environ.-Res.-Lett., 16 043005, <https://doi.org/10.1088/1748-9326/abed00>, 2021.

1271 Webb, J.R., Leavitt, P.R., Simpson, G.L., Baulch, H.M., Haig, H.A., Hodder, K.R., and Finlay, K.: Regulation of carbon
1272 dioxide and methane in small agricultural reservoirs: optimizing potential for greenhouse gas uptake.
1273 *Biogeosciences*, 16 (21), 4211–4227. <https://doi.org/10.5194/bg-16-4211-2019>, 2019.

1274 Webb, J.R., Quayle, W.C., Ballester, C., Wells, N.: Semi-arid irrigation farm dams are a small source of greenhouse gas
1275 emissions. *Biogeochemistry*, 166, 123–138. <https://doi.org/10.1007/s10533-023-01100-4>, 2023.

1276 Weiss, R. F., Price, B. A.: Nitrous oxide solubility in water and seawater. *Marine chemistry*, 8(4), 347-359.,
1277 [doi.org/10.1016/0304-4203\(80\)90024-9](https://doi.org/10.1016/0304-4203(80)90024-9), 1980.

1278 Weiss, R. F.: Determinations of carbon dioxide and methane by dual catalyst flame ionization chromatography and nitrous
1279 oxide by electron capture chromatography. *Journal of Chromatographic Science, J.-Chromatogr.-Sci.* 19, 611–616.
1280 <https://doi.org/10.1093/chromsci/19.12.611>, 1981.

1281 West, W.E., Coloso, J.J., and Jones, S.E.: Effects of algal and terrestrial carbon on methane production rates and methanogen
1282 community structure in a temperate lake sediment. *Freshwater Biology*, 57, 949–955.
1283 <https://doi.org/10.1111/j.1365-2427.2012.02755.x>, 2012.

1284 Wik, M., Crill, P. M., Varner, R. K., and Bastviken, D.: Multiyear measurements of ebullitive methane flux from three
1285 subarctic lakes. *Journal of Geophysical Research: Biogeosciences*, *J. Geophys. Res. Biogeosciences* 118:791 1307–
1286 1321. <https://doi.org/10.1002/jgrg.20103>, 2013.

1287 Xie, S., T Xia, T., H Li, H., Y Chen, Y., W Zhang, W. , 2024, Variability in N2O emission controls among different ponds
1288 within a hilly watershed, *Water Research*, 267, 122467, <https://doi.org/10.1016/j.watres.2024.122467>, 2024.

1289 Xun, F., Feng, M., Ma, S., Chen, H., Zhang, W., Mao, Z., Zhou, Y., Xiao, Q, Wu, Q. L., and Xing, P.: Methane ebullition
1290 fluxes and temperature sensitivity in a shallow lake. *Science of The Total Environment*, 912, 169589.
1291 <https://doi.org/10.1016/j.scitotenv.2023.169589>, 2024.

1292 Yan, X., Xu, X., Ji, M., Zhang, Z., Wang, M., Wu, S., Wang, G., Zhang, C., and Liu, H.: Cyanobacteria blooms: A neglected
1293 facilitator of CH4 production in eutrophic lakes. *Science of the total environment*, 651, 466-474.
1294 <https://doi.org/10.1016/j.scitotenv.2018.09.197>, 2019.

1295 Yang, Z., Zhao, Y., and Xia, X.: Nitrous oxide emissions from Phragmites australis-dominated zones in a shallow lake.
1296 *Environmental pollution*, 166, 116-124. <https://doi.org/10.1016/j.envpol.2012.03.006>, 2012.

1297 Yentsch, C.S., and Menzel, D.W.: A method for the determination of phytoplankton chlorophyll and phaeophytin by
1298 fluorescence.—In: *Deep Sea Research and Oceanographic Abstracts*, 10. Elsevier, pp. 221–231.
1299 [https://doi.org/10.1016/0011-7471\(63\)90358-9](https://doi.org/10.1016/0011-7471(63)90358-9), 1963.

1300 Zhao, K., Tedford, E.W., Zare, M., and Lawrence, G.A.: Impact of atmospheric pressure variations on methane ebullition
1301 and lake turbidity during ice - cover. *Limnology and Oceanography Letters*, 6(5), 253-261.
1302 <https://doi.org/10.1002/lol2.10201>, 2021.

1303